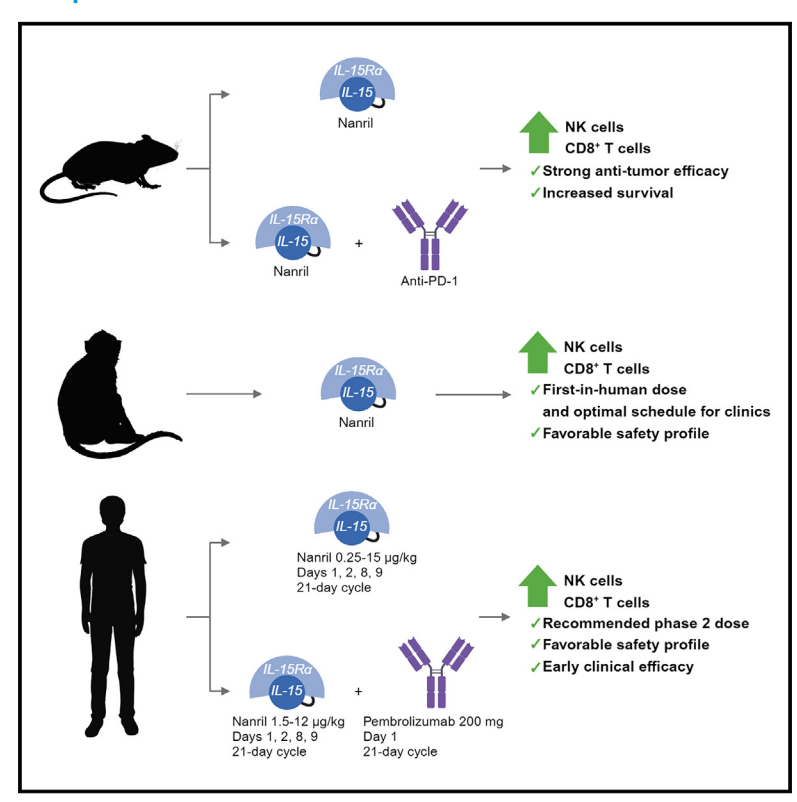
# Nanrilkefusp alfa (SOT101), an IL-15 receptor $\beta\gamma$ superagonist, as a single agent or with anti-PD-1 in patients with advanced cancers

#### **Graphical abstract**



#### **Authors**

Stephane Champiat, Elena Garralda, Vladimir Galvao, ..., Lenka Palova Jelinkova, Irena Adkins, Aurelien Marabelle

#### Correspondence

schampiat@mdanderson.org

#### In brief

Champiat et al. report that nanrilkefusp alfa, an IL-15R $\beta\gamma$  superagonist, showed strong anti-tumor activity and increased survival in mice. The dose and dosing schedule for the clinics were established in cynomolgus monkeys. In patients, favorable safety and early clinical efficacy were observed in monotherapy and in combination with pembrolizumab.

#### **Highlights**

- Nanrilkefusp alfa is an IL-15R $\beta\gamma$  superagonist stimulating NK and CD8<sup>+</sup> T cells
- In mice, nanril showed strong anti-tumor activity and increased survival
- In cynomolgus monkeys, the dose and schedule were established for the clinics
- In patients, a favorable safety profile and early clinical benefit were observed







#### **Article**

# Nanrilkefusp alfa (SOT101), an IL-15 receptor $\beta\gamma$ superagonist, as a single agent or with anti-PD-1 in patients with advanced cancers

Stephane Champiat, <sup>1,13,15,\*</sup> Elena Garralda, <sup>2</sup> Vladimir Galvao, <sup>2</sup> Philippe A. Cassier, <sup>3</sup> Carlos Gomez-Roca, <sup>4</sup> Iphigenie Korakis, <sup>4</sup> Peter Grell, <sup>5</sup> Aung Naing, <sup>6</sup> Patricia LoRusso, <sup>7</sup> Romana Mikyskova, <sup>8</sup> Nada Podzimkova, <sup>9</sup> Milan Reinis, <sup>8</sup> Kaissa Ouali, <sup>1</sup> Andreu Schoenenberger, <sup>9</sup> Joachim Kiemle-Kallee, <sup>10</sup> Sascha Tillmanns, <sup>10</sup> Richard Sachse, <sup>10</sup> Ulrich Moebius, <sup>9</sup> Radek Spisek, <sup>9</sup> David Bechard, <sup>11</sup> Lenka Palova Jelinkova, <sup>9,12,14</sup> Irena Adkins, <sup>9,12,14</sup> and Aurelien Marabelle<sup>1,14</sup>

#### **SUMMARY**

Nanrilkefusp alfa (nanril; SOT101) is an interleukin (IL)-15 receptor  $\beta\gamma$  superagonist that stimulates natural killer (NK) and CD8<sup>+</sup> T cells, thereby promoting an innate and adaptive anti-tumor inflammatory microenvironment in mouse tumor models either in monotherapy or combined with an anti-programmed cell death protein 1 (PD-1) antibody. In cynomolgus monkeys, a clinical schedule was identified, which translated into the design of a phase 1/1b clinical trial, AURELIO-03 (NCT04234113). In 51 patients with advanced/metastatic solid tumors, nanril increased the proportions of CD8<sup>+</sup> T cells and NK cells in peripheral blood and tumors. It had a favorable safety profile when administered subcutaneously on days 1, 2, 8, and 9 of each 21-day cycle as monotherapy (0.25–15  $\mu$ g/kg) or combined (1.5–12  $\mu$ g/kg) with the anti-PD-1 pembrolizumab (200 mg). The most frequent treatment-emergent adverse events were pyrexia, injection site reactions, and chills. Furthermore, early clinical efficacy was observed, including in immune checkpoint blockade-resistant/refractory patients.

#### **INTRODUCTION**

Interleukin-15 (IL-15) is one of the most promising cytokines for cancer immunotherapy.  $^1$  Compared to high-dose IL-2,  $^{2,3}$  IL-15 and IL-2/IL-15 receptor (R)  $\beta\gamma$  agonists showed a better safety profile.  $^{4-8}$  Not only does IL-15 activate natural killer (NK) cells, NKT cells,  $\gamma\delta$  T cells, and CD8+ T cells, it also stimulates and maintains memory CD8+ T cell responses,  $^9$  does not cause activation-induced cell death,  $^{10}$  and has low effect on regulatory T cell (Treg) expansion.  $^{11}$ 

Nanrilkefusp alfa (nanril; SOT101, formerly RLI-15 or SOC101) is a fusion protein comprising the N-terminal sushidomain of human IL-15R $\alpha$  covalently coupled via a glycineserine linker to human IL-15.  $^{12,13}$  Nanril selectively binds to IL-2/IL-15R $\beta\gamma$  with high affinity, thereby inducing the proliferation and activation of CD8 $^+$ T cells, memory CD8 $^+$ T cells, NK cells,  $\gamma\delta$ T cells, and NKT cells in vitro and in vivo without stimulating Treg expansion.  $^{14-18}$  Nanril demonstrated stronger anti-tumor and anti-metastatic activity than IL-15 in mouse cancer models.  $^{16,17,19}$  Nanril was also shown to improve survival when



<sup>&</sup>lt;sup>1</sup>Gustave Roussy, Departement d'Innovation Therapeutique et d'Essais Precoces (DITEP), Universite Paris Saclay, 94805 Villejuif, France

<sup>&</sup>lt;sup>2</sup>Vall d'Hebron Institute of Oncology, 08035 Barcelona, Spain

<sup>&</sup>lt;sup>3</sup>Department of Medical Oncology, Centre Leon Berard, 69008 Lyon, France

<sup>&</sup>lt;sup>4</sup>Institut Universitaire du Cancer de Toulouse, 31100 Toulouse, France

<sup>&</sup>lt;sup>5</sup>Masaryk Memorial Cancer Institute, 602 00 Brno, Czech Republic

<sup>&</sup>lt;sup>6</sup>Department of Lnvestigational Cancer Therapeutics, MD Anderson Cancer Center, Houston, TX 77030, USA

<sup>&</sup>lt;sup>7</sup>Yale School of Medicine, New Haven, CT 06510, USA

<sup>&</sup>lt;sup>8</sup>Laboratory of Immunological and Tumor Models, Institute of Molecular Genetics of the Czech Academy of Sciences, 142 20 Prague, Czech Republic

<sup>&</sup>lt;sup>9</sup>SOTIO Biotech a.s., 170 00 Prague, Czech Republic

<sup>&</sup>lt;sup>10</sup>SOTIO Biotech AG, 4056 Basel, Switzerland

<sup>&</sup>lt;sup>11</sup>Cytune Pharma, 44300 Nantes, France

<sup>&</sup>lt;sup>12</sup>Department of Immunology, 2nd Faculty of Medicine and University Hospital Motol, Charles University, 150 06 Prague, Czech Republic

<sup>&</sup>lt;sup>13</sup>Present address: Department of Investigational Cancer Therapeutics, Division of Cancer Medicine, The University of Texas MD Anderson Cancer Center, Houston, Texas, USA

<sup>&</sup>lt;sup>14</sup>Senior authors

<sup>15</sup>Lead contact

<sup>\*</sup>Correspondence: schampiat@mdanderson.org https://doi.org/10.1016/j.xcrm.2025.101967



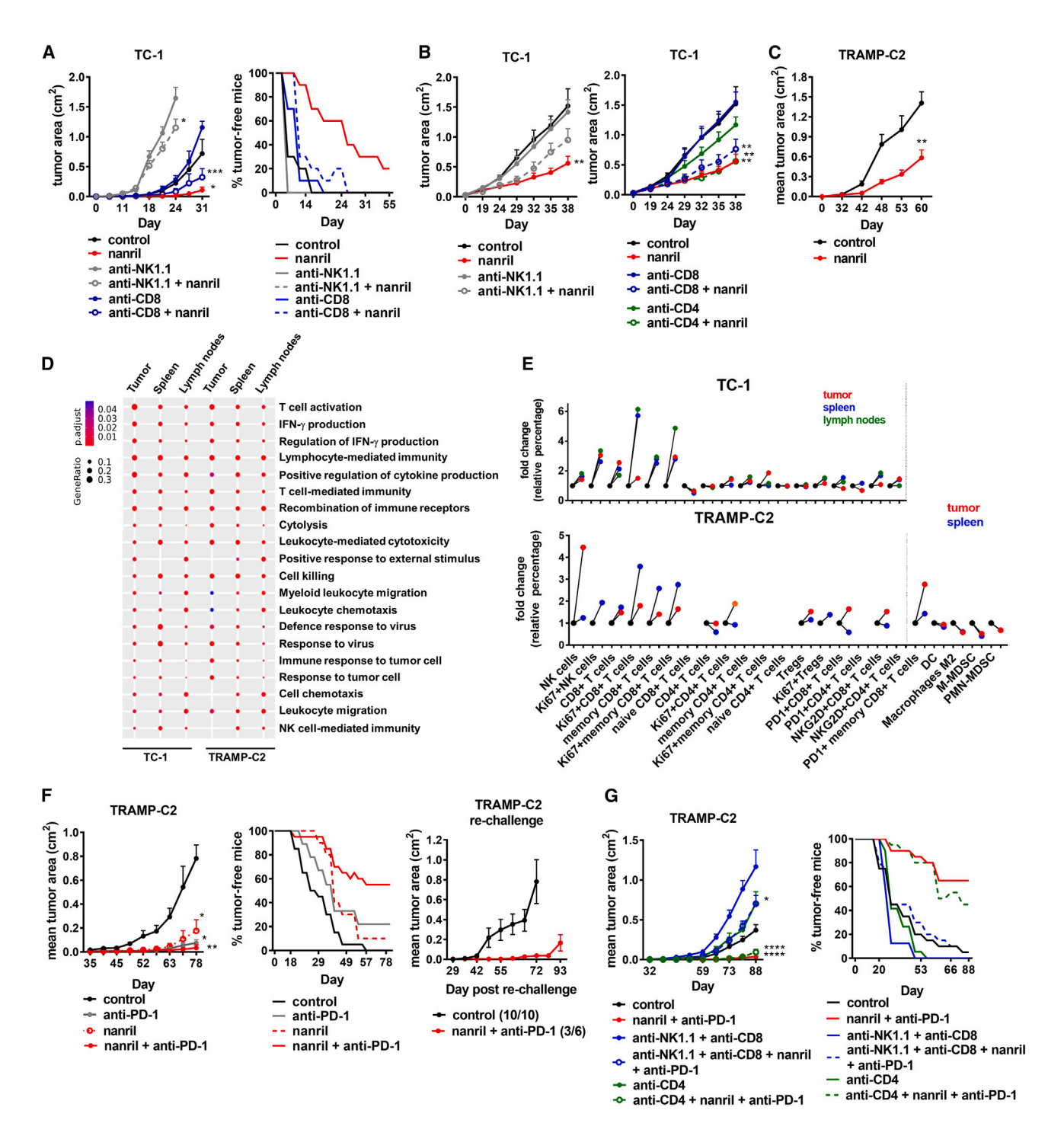


Figure 1. Nanril as monotherapy or combined with an anti-PD-1 antibody induces strong NK and CD8<sup>+</sup> T cell-dependent anti-tumor efficacy and induces an inflammatory tumor microenvironment

(A)  $3 \times 10^4$  TC-1 cells were implanted s.c. in C57BL/6 mice on day 0. TC-1 tumor-bearing mice were treated s.c. with nanril at 2 mg/kg once daily on days 4–7 and 10–13 post inoculation. Antibodies to deplete NK/CD8+/CD4+ T cells were administered intraperitoneally (i.p.) on days -7, -4, -2, 4, 11, and 18. Depletion of NK cells markedly accelerated TC-1 tumor growth (there were no tumor-free mice at day 7).

(B)  $3 \times 10^4$  TC-1 cells were implanted s.c. in C57BL/6 mice on day 0. Mice were treated s.c. with nanril at 2 mg/kg once daily on days 25–28 and 32–35 (day 25 randomization  $\sim$ 0.1 cm<sup>2</sup>). Antibodies to deplete NK/CD8+/CD4+ T cells were administered i.p. on days 21, 24, 26, and 33.

(C)  $1 \times 10^6$  TRAMP-C2 cells were implanted s.c. in C57BL/6 mice on day 0. Mice were treated s.c. with nanril at 1 mg/kg once daily on days 36–39 and 50–53 (day 36 randomization  $\sim$ 0.1 cm<sup>2</sup>) or with vehicle alone as a control.

#### **Article**



combined with an anti-programmed cell death protein (PD-1) antibody in mouse colorectal carcinoma models, displaying superiority over an anti-PD-1 antibody combined with IL-15. <sup>16</sup> Here, the effect of nanril was dependent on CD8<sup>+</sup> T cell-mediated immunity. Immune checkpoint blockers (ICBs) targeting PD-1 or its ligand (programmed cell death ligand 1 [PD-L1]) have become a standard of care for many advanced solid malignancies. <sup>20,21</sup> However, most patients do not show long-term benefit from anti-PD-1 monotherapy due to primary or secondary resistance, in particular, a limited number of tumor-infiltrating anti-tumor effector lymphocytes. <sup>22–25</sup> Therefore, combined anti-PD(L)1 immunotherapy with nanril represents a complementary strategy to achieve effective and long-lasting anti-tumor immune responses by mobilizing and expanding anti-tumor effector lymphocytes.

We investigated the underlying contributions of the target immune cells in anti-tumor efficacy mediated by nanril when administered as monotherapy or combined with an anti-PD-1 antibody in subcutaneous lung human papillomavirus 16 E6/E7 expressing TC-1 and prostate TRAMP-C2 mouse tumor models. We further evaluated the pharmacodynamics (PD), pharmacokinetics (PK), and safety of nanril in cynomolgus monkeys to predict the optimal clinical dosing schedule. Based on the encouraging pre-clinical results, we conducted a phase 1/1b clinical trial (AURELIO-03, NCT04234113), in which patients with selected advanced/metastatic solid tumors were administered nanril subcutaneously (s.c.) as monotherapy or combined with the anti-PD-1 pembrolizumab.

#### **RESULTS**

# Nanril as monotherapy or combined with an anti-PD-1 antibody induces strong NK and CD8<sup>+</sup> T cell-dependent anti-tumor efficacy and an inflammatory tumor microenvironment

The anti-tumor efficacy and the activation of NK and CD8<sup>+</sup> T cells and their regulating pathways were investigated in the TC-1 and TRAMP-C2 mouse models. These models have the advantage of looking at innate as well as adaptive immune responses in the anti-tumor response, in contrast to other, mostly CD8<sup>+</sup> T cell response polarized, preclinical mouse models. Nanril monotherapy significantly slowed tumor development in an early therapeutic setting of the TC-1 model (Figure 1A). Specific depletion of immune cell subsets illustrated that this effect was mainly

dependent on NK and CD8<sup>+</sup> T cells. Late-stage treatment of established tumors significantly decreased the kinetics of tumor growth in both models (Figures 1B and 1C). Only NK cell depletion abrogated the effect of nanril at this stage (Figure 1B). Nanril activated signaling pathways connected to anti-tumor immunity, cell migration, and proinflammatory cytokine production in the tumors, spleens, and lymph nodes in both models (Figures 1D, \$1A, and \$1B). Genes associated with NK cell functional cytotoxicity and genes determining the increased relative abundance of CD8+ T cells, NK cells, and cytotoxic cells were upregulated (Figures S1B and S1C). Nanril increased the relative abundance and proliferation of NK cells and CD8<sup>+</sup> and memory CD8<sup>+</sup> T cells in the tumors, spleens, and lymph nodes in both models (Figure 1E). Of note, CD4<sup>+</sup> T cells and Tregs were expanded less effectively (Figure 1E). Interestingly, nanril decreased the relative percentage of suppressive myeloid cells and M2 macrophages in TRAMP-C2 tumors (Figure 1E).

In TRAMP-C2 tumors, nanril increased the relative percentage of PD-1<sup>+</sup>CD8<sup>+</sup> T cells (Figure 1E). Therefore, we investigated the anti-tumor efficacy of nanril combined with an anti-PD-1 antibody and the underlying immune cell involvement in TRAMP-C2 tumors. Nanril combined sequentially with an anti-PD-1 antibody prevented tumor development in 60% of mice (Figure 1F). A similar effect occurred when both drugs were used concomitantly (Figure S2A). Tumor development was delayed after tumor re-challenge in 50% of the cured mice, suggesting an involvement of memory T cells, despite the important role of NK cells in the anti-tumor efficacy of nanril in the TRAMP-C2 model (Figure 1F). Both NK and CD8+ T cells were important to the nanriland anti-PD-1-mediated anti-tumor responses (Figure S2B). Interestingly, combined nanril and anti-PD-1 treatment significantly decreased tumor growth and development in double-NK/CD8<sup>+</sup> T cell-depleted mice, indicating that other immune cell populations also contribute to the anti-tumor efficacy (Figure 1G). These data demonstrate the importance of several target immune cell populations stimulated by nanril as monotherapy or combined with an anti-PD-1 antibody.

# Subcutaneous administration of nanril on days 1, 2, 8, and 9 was selected as an optimal clinical schedule based on cynomolgus monkey studies

The dose, route of administration, PD, and PK of nanril were investigated in cynomolgus monkey studies. PD parameters were assessed on day 5 after once-daily s.c. or intravenous

Data represent the mean  $\pm$  SEM of n=2–3 or one representative experiment (8–10 mice per group). \*p<0.05, \*\*p<0.01, \*\*\*p<0.001, and \*\*\*\*\*p<0.001 (one-way ANOVA or unpaired Mann-Whitney test). DCs, dendritic cells; M-MDSCs, monocytic myeloid-derived suppressor cells; ns, not significant; PMN-MDSCs, polymorphonuclear myeloid-derived suppressor cells.

See also Figures S1 and S2.

<sup>(</sup>D) Gene Ontology enrichment analysis of the differentially expressed genes in the tumors, spleens, and lymph nodes collected 5 days after the start of treatment with nanril was determined by NanoString nCounter analysis (n = 5, 2 independent experiments).

<sup>(</sup>E) Fold change in the relative percentage of specific immune cell populations, as detected by flow cytometry, in the tumors, spleens, and lymph nodes collected 5 days after starting nanril treatment. Values in control untreated samples were set to 1, and the relative percentage for untreated tumors was set to 1 (samples spleen, lymph nodes, and tumors n = 3-5, 2 independent experiments).

<sup>(</sup>F) TRAMP-C2-bearing mice were treated s.c. with nanril at 1 mg/kg once daily on days 4–7 and 18–21 either alone or combined with an anti-PD-1 antibody at 12.5 mg/kg i.p. on days 10, 13, and 16. Nanril combined with an anti-PD-1 antibody significantly delayed tumor development in cured mice after re-challenge with TRAMP-C2 tumor cells on day 106 post treatment (6–10 mice/group).

<sup>(</sup>G) TRAMP-C2-tumor bearing mice were treated s.c. as in (F). Antibodies for depleting NK/CD8+/CD4+ T cells were administered on days -7, -4, -2, 4, 11, and 18.



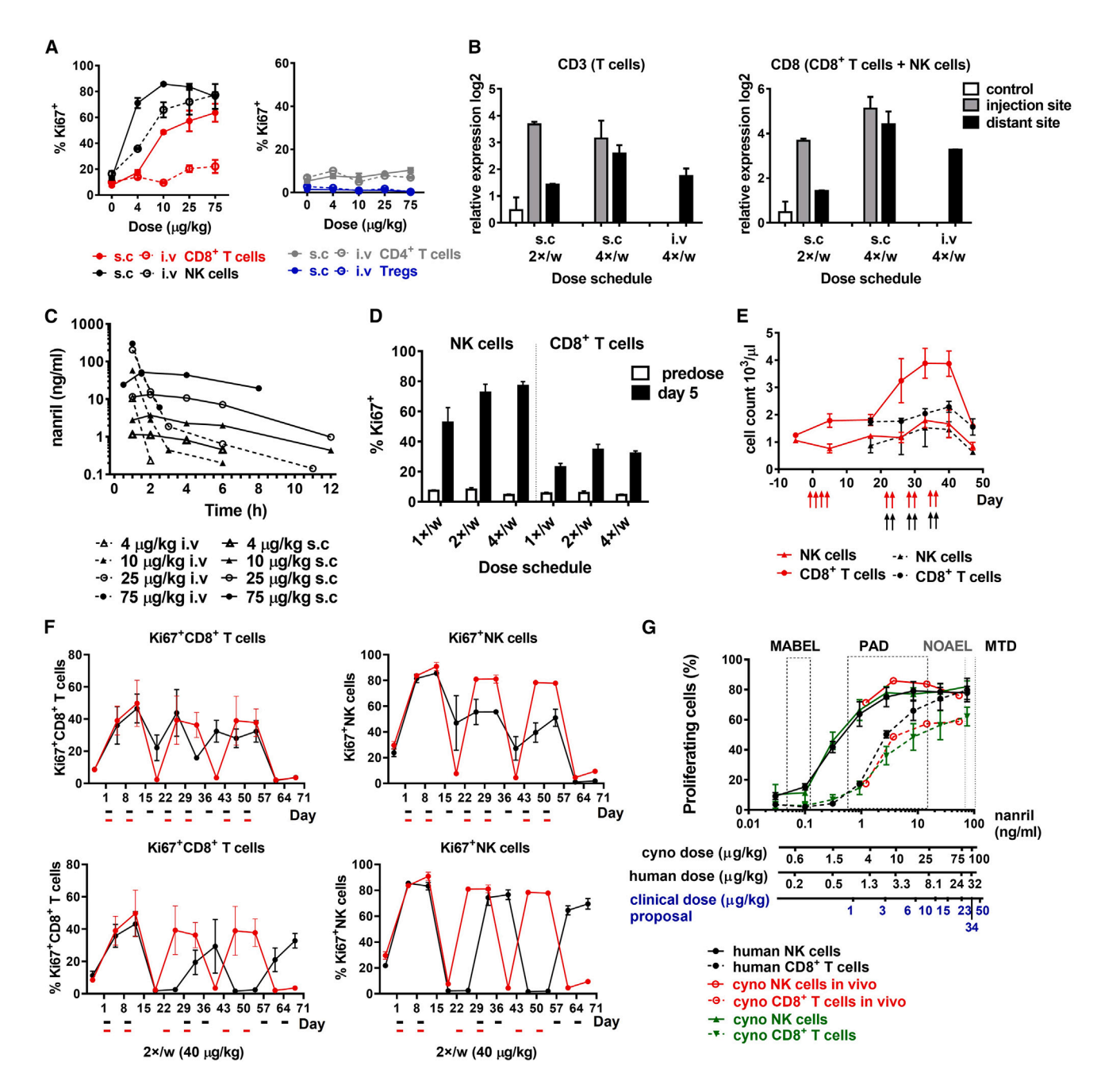


Figure 2. Nanril administered s.c. on days 1, 2, 8, and 9 was selected as the optimal clinical schedule based on cynomolgus monkey studies (A) s.c. administration of nanril for 4 consecutive days induced greater proliferation of NK and CD8<sup>+</sup> T cells on day 5 compared with i.v. administration (infusion over 60 min). No CD4<sup>+</sup> T cell or Treg proliferation was detected by flow cytometry of peripheral blood mononuclear cells from cynomolgus monkeys. (B) qPCR analysis of immune cells expressing CD3<sup>-</sup>- and CD8a-related genes from skin biopsies. The skin biopsy was collected at the injection site and at a distant site from 8 days after the last dose (group s.c. 4×/w at 15 μg/kg and i.v. 4×/w at 40 μg/kg) and 2 days after the last dose (group s.c. 2×/w at 15 μg/kg). Biopsies from untreated (NT) monkeys not related to the study were used as the control.

- (C) PK profiles of nanril upon s.c. and i.v. administration. Serum was collected at the indicated time points and analyzed by ELISA.
- (D) Four (days 1–4;  $4 \times /w$ ) or two (days 1, 2;  $2 \times /w$ ) s.c. doses of nanril at 15  $\mu$ g/kg induced similar proliferation of NK and CD8<sup>+</sup> T cells on day 5, exceeding that achieved by a single (day 1;  $1 \times /w$ ) s.c. administration.
- (E) Immune cell activation during 3 weeks of nanril administration (days 22, 23, 29, 30, 36, and 37). An additional s.c. dose of nanril at 15  $\mu$ g/kg at days 36 and 37 did not further increase the proliferation of NK or CD8<sup>+</sup>T cells, regardless of the previous nanril treatment. Arrows represent dosing schedule; colors correspond to the immune cells in the graph and the dosing.
- (F) s.c. administration of nanril at 40  $\mu$ g/kg in 21-day cycles (days 1, 2, 8, and 9 + 1 week off-treatment) (red dosing schedule below graphs) induced greater proliferation of NK cells, but not CD8<sup>+</sup> T cells, compared with two administrations every week (days 1, 2, 8, 9, 15, 16 etc.) (black dosing schedule below graphs) in a

#### **Article**



(i.v.) administration on days 1, 2, 3, and 4. NK and CD8<sup>+</sup> T cell proliferation was stronger after s.c. compared with i.v. administration, whereas the proliferation of Tregs and CD4<sup>+</sup> T cells was low (Figure 2A). To investigate the PD after s.c. administration in tissues, we performed qPCR of CD3<sup>-</sup>- and CD8a-related genes using monkey skin biopsies. The upregulation of NK and CD8<sup>+</sup> T cell-related genes in the skin was greater following s.c. than i.v. administration at a biopsy site distant from the administration site (Figure 2B). The PK indicated greater, dose-dependent exposure after s.c. compared with i.v. administration (Figure 2C; Table S1). The bioavailability after s.c. administration ranged from 35% (10 and 25  $\mu$ g/kg) to 47% (4  $\mu$ g/kg). The half-life for s.c. administration was 3–4 h and was consistent over the doses tested.

We also compared the PD on day 5 after once-daily s.c. administration for 1, 2, or 4 consecutive days (Figure 2D). Nanril administered s.c. induced similarly high proliferation of NK and CD8 $^+$  T cells on day 5 for 4 (days 1–4; 4×/w) or 2 (days 1 and 2; 2×/w) consecutive days. Cell proliferation was lower after a single dose (day 1; 1×/w) than after multiple doses.

The 2x/w regimen was selected to investigate the number of consecutive dosing weeks required for optimal PD (Figure 2E). Nanril s.c. administration at 2x/w for 2 consecutive weeks achieved the greatest PD, and an additional s.c. dose in week 3 did not increase NK and CD8+ T cell proliferation, regardless of the prior dosing (Figure 2E). To assess the suitability of the 2x/w schedule as a 21-day cycle for the clinical trial, we performed a 10-week study in cynomolgus monkeys. Nanril administered s.c. on days 1, 2, 8, and 9 with a 1-week off-treatment period (21-day cycle) increased NK cell proliferation, but not CD8<sup>+</sup> T cell proliferation, compared with continuous dosing (Figure 2F). This was not reflected in the NK cell counts (Figure S3) because a higher NK cell count was observed for the continuous schedule. One-week or 2-week off-treatment periods did not affect the magnitude of NK and CD8+ T cell proliferation (Figure 2F). This suggested that a 1-week off-treatment period is sufficient for the immune cells to regain their full proliferative potential similar to previous treatment cycles.

Nanril showed a good correlation in inducing NK and CD8<sup>+</sup> T cell proliferation *in vitro* in human (EC<sub>50</sub>; NK, 13.8 pM; CD8<sup>+</sup>, 86.9 pM) and cynomolgus monkey (EC<sub>50</sub>; NK, 12.7 pM; CD8<sup>+</sup>, 104 pM) cells (Figure 2G). Similar proliferation of NK and CD8<sup>+</sup> T cells was observed in cynomolgus monkeys *in vivo* (Figure 2G).

Nanril was well tolerated in cynomolgus monkeys up to 80  $\mu$ g/kg (4×/w s.c. administration for 4 weeks). The no-observed-adverse-effect level was 80  $\mu$ g/kg. The maximum tolerated dose (MTD) was observed at 100  $\mu$ g/kg using a similar dosing schedule. Based on the minimum anticipated biological effect level, receptor occupancy, and allometric scaling, the proposed effective human dose range was 1–50  $\mu$ g/kg (Figure 2G).

#### Nanril was well tolerated in human patients with cancer

Fifty-one patients with advanced/metastatic solid tumors received nanril as monotherapy or combined with pembrolizumab in a first-in-human phase 1/1b clinical trial (AURELIO-03, NCT04234113; Figure S4). Final monotherapy data and combination data collected at the data cutoff (September 2022) are reported here. In the monotherapy part, 30 patients were treated at nanril doses ranging from 0.25 to 15  $\mu g/kg$ . In the combination part, 21 patients were treated at nanril doses ranging from 1.5 to 12  $\mu g/kg$  combined with 200 mg pembrolizumab. Nanril was administered s.c. on days 1, 2, 8, and 9, and pembrolizumab was administered i.v. on day 1 of each 21-day cycle.

Patients with a variety of advanced tumors were enrolled; the most common histologic types were biliary tract, skin, bladder, and ovary (Table S2). A higher proportion of patients in the monotherapy part (53.3%) than in the combination part (38.1%) had an Eastern Cooperative Oncology Group performance status of 1. The median (range) number of previous anti-cancer treatment lines was 3 (1–9) and 2 (1–6) in the monotherapy and combination parts, respectively. In the monotherapy part, 19 patients (63.3%) were previously treated with ICBs, of whom 9 (47.4%) were refractory and 5 (26.3%) had relapsed. In the combination part, 12 patients (57.1%) had prior exposure to ICBs, of whom 1 (8.3%) was refractory and 9 (75.0%) had relapsed disease. Other baseline characteristics were similar between the treatment groups (Table S2).

In the monotherapy part, no dose-limiting toxicities (DLTs) occurred at doses up to 12  $\mu g/kg$ . At 15.0  $\mu g/kg$ , 2 DLTs occurred; both were increased liver function tests: one was grade 3 alanine aminotransferase (ALT) and aspartate aminotransferase (AST) elevations (the patient continued at 9  $\mu g/kg$  until the end of cycle 3), and the other was grade 4 bilirubin with grade 3 ALT and AST elevations. Both events quickly improved to grade  $\leq 1$  after dose reduction or nanril discontinuation. In the combination part, one DLT (grade 3 cytokine release syndrome with symptoms of grade 3 hypotension, grade 2 oliguria and grade 2 rash; all resolved within 2 days) occurred at 6.0  $\mu g/kg$ ; none occurred at 9.0 and 12  $\mu g/kg$ . Based on the safety and PK and PD data, the recommended phase 2 dose of nanril as monotherapy or combined with pembrolizumab was defined as 12  $\mu g/kg$ .

All 51 treated patients experienced at least one treatment-emergent adverse event (TEAE). The most frequent TEAEs for monotherapy vs. combination therapy were pyrexia (70.0% vs. 81.0% of patients), injection site reactions (60.0% vs. 81.0%), and chills (50.0% vs. 71.4%; Table 1). Most TEAEs were of grade 1 or 2 (Table 1; Figure S5). The most frequent grade 3 or 4 TEAE was a transient decrease in lymphocyte count. No grade 5 TEAEs related to the study treatment were observed. Nanril was permanently discontinued due to TEAEs in 4 (13.3%) and 2 (9.5%) patients in the monotherapy and combination parts, respectively. The

10-week scheduling study in cynomolgus monkeys. The magnitude of cell proliferation did not differ when nanril was administered with a 1-week (red dosing schedule below graphs) or 2-week (black dosing schedule below graph) off-treatment period during the course of the study. Treatment days/schedule are represented by bars; line color corresponds to treatment schedule.

(G) The proliferation of human and cynomolgus monkey NK and CD8<sup>+</sup> T cells *in vitro* showed similar patterns (Ki67<sup>+</sup>) to that observed *in vivo* in cynomolgus monkeys, as determined by flow cytometry. Cell counts were determined by using the percentages of a population within CD45<sup>+</sup> cells obtained by flow cytometry and the white blood cell count from hematologic analysis.

All studies comprised a mean  $\pm$  SEM of 2 animals per group.

See also Figure S3; Table S1.



	Monotherapy (N = 30)		Combination (N = 21)		All patients (N = 51)	
TEAE -						
	All	Grade ≥3	All	Grade ≥3	All	Grade ≥3
Any TEAE	30 (100.0)	25 (83.3)	21 (100.0)	17 (81.0)	51 (100.0)	42 (82.4)
Pyrexia	21 (70.0)	1 (3.3)	17 (81.0)	3 (14.3)	38 (74.5)	4 (7.8)
Injection site reaction	18 (60.0)	0	17 (81.0)	0	35 (68.6)	0
Chills	15 (50.0)	0	15 (71.4)	0	30 (58.8)	0
Lymphocyte count decreased	20 (66.7)	19 (63.3)	10 (47.6)	8 (38.1)	30 (58.8)	27 (52.9)
Anemia	17 (56.7)	3 (10.0)	11 (52.4)	2 (9.5)	28 (54.9)	5 (9.8)
AST increased	13 (43.3)	2 (6.7)	12 (57.1)	2 (9.5)	25 (49.0)	4 (7.8)
ALT increased	12 (40.0)	2 (6.7)	11 (52.4)	2 (9.5)	23 (45.1)	4 (7.8)
Vomiting	10 (33.3)	0	11 (52.4)	0	21 (41.2)	0
Nausea	8 (26.7)	0	11 (52.4)	0	19 (37.3)	0
Asthenia	12 (40.0)	1 (3.3)	5 (23.8)	1 (4.8)	17 (33.3)	2 (3.9)
Fatigue	8 (26.7)	0	7 (33.3)	0	15 (29.4)	0
Hypotension	7 (23.3)	0	8 (38.1)	0	15 (29.4)	0
Alkaline phosphatase increased	7 (23.3)	1 (3.3)	5 (23.8)	1 (4.8)	12 (23.5)	2 (3.9)
Diarrhea	6 (20.0)	1 (3.3)	6 (28.6)	0	12 (23.5)	1 (2.0)
Tumor pain	10 (33.3)	1 (3.3)	2 (9.5)	0	12 (23.5)	1 (2.0)
Blood creatinine increased	5 (16.7)	0	6 (28.6)	0	11 (21.6)	0
Decreased appetite	8 (26.7)	2 (6.7)	3 (14.3)	0	11 (21.6)	2 (3.9)
Abdominal pain	7 (23.3)	0	3 (14.3)	0	10 (19.6)	0
Gamma-glutamyltransferase increased	4 (13.3)	1 (3.3)	6 (28.6)	2 (9.5)	10 (19.6)	3 (5.9)
Headache	5 (16.7)	0	5 (23.8)	0	10 (19.6)	0
Bilirubin increased	5 (16.7)	1 (3.3)	4 (19.0)	0	9 (17.6)	1 (2.0)
Lipase increased	4 (13.3)	1 (3.3)	4 (19.0)	1 (4.8)	8 (15.7)	2 (3.9)
Neutrophil count decreased	4 (13.3)	2 (6.7)	4 (19.0)	2 (9.5)	8 (15.7)	4 (7.8)
Values are n (%) of patients						

ALT, alanine aminotransferase; AST, aspartate aminotransferase; TEAE, treatment-emergent adverse event. See also Figure S5.

most frequent TEAEs leading to treatment discontinuation were asthenia and decreased appetite (2 patients, 6.7%) in the monotherapy part, and transaminase increase and cytokine release syndrome (1 patient each, 4.8%) in the combination part.

# Nanril showed dose-proportional exposure in monotherapy and combined with pembrolizumab in human patients with cancer

Dose-proportional exposure was observed, and the maximum serum concentration of nanril was reached 4–8 h after s.c. administration. The mean terminal half-life after the first dose was around 4 h across all doses in the monotherapy and combination parts. Overall, the PK profile was comparable between the monotherapy and combination parts (Figure S6).

# Nanril showed promising anti-tumor activity in monotherapy and combined with pembrolizumab in human patients with cancer

The median follow-up was 13.3 months and 8.3 months (ongoing) in the monotherapy and combination parts of AURELIO-03, respectively. One patient (3.3%) initially in the

monotherapy part and 6 patients (28.6%) in the combination part were still on treatment with pembrolizumab combination at data cutoff (Figure 3). Efficacy is reported here as the overall (best) Immune-related Response Evaluation Criteria in Solid Tumors (iRECIST) objective response rate (ORR) and disease control rate (DCR).

In the monotherapy efficacy population (n=26), a confirmed iRECIST partial response (PR) was observed in 1 patient (3.8%) (Figure 4A). This patient had metastatic skin squamous cell carcinoma (sSCC) refractory to cemiplimab (anti-PD-1) and was treated with nanril at 6  $\mu$ g/kg. After 4 months on nanril monotherapy (6 months after the last cemiplimab infusion), the patient relapsed and was crossed over to the combination part. On combination therapy, this patient again developed a clinical response (Figure 4A), a partial iRECIST CT-scan response (Figure 4A), and a complete metabolic response (Figure 4B). Peripheral blood PD analysis showed that nanril alone or combined with pembrolizumab stimulated the proliferation of NK cells, NKT cells, and CD8+ T cells, but not Tregs. Contrary to NKT and CD8+ T cell proliferation, which peaked in cycle 1 and then slightly dropped, high NK cell proliferation was maintained over 3 cycles of both

#### **Article**



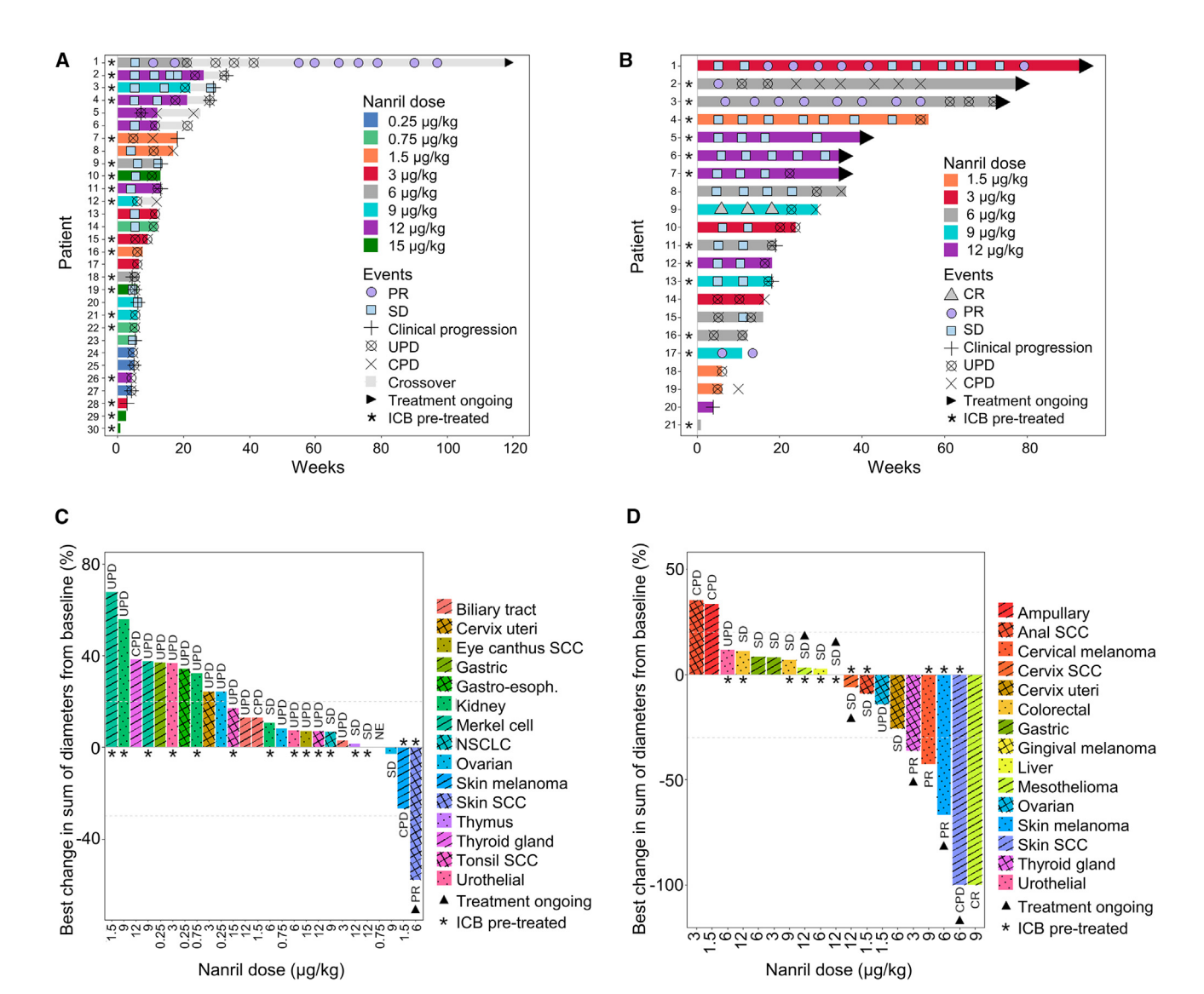


Figure 3. Anti-tumor efficacy of nanril in patients with advanced/metastatic solid tumors
(A and B) Swimmer plots of time on treatment in the monotherapy part (A) and in the combination part (B).
(C and D) Waterfall plots of the best percent change in tumor size from baseline in the monotherapy part (C) and in the combination part (D).

monotherapy and combination therapy (Figure S7A). The frequency of PD1<sup>+</sup>CD8<sup>+</sup> T cells in peripheral blood was also increased by nanril monotherapy (Figure S7B). The tumor biopsy sample taken at baseline and at the time of the nanril relapse showed increased densities of CD3<sup>+</sup>, CD4<sup>+</sup>, and CD8<sup>+</sup> tumor-infiltrating lymphocytes (TILs), proliferating TILs, and NK cells, as well as a significant increase in PD-L1<sup>+</sup> cells and increased Tregs in the relapse biopsy compared to baseline (Figures S7C and S7D). Expression of genes associated with T helper 1 (Th1) and NK cell activation and cytotoxicity, as well as several immune checkpoints including PD-L1, PD-L2, PD-1, T cell immunoglobulin and mucin domain-containing protein 3 (TIM-3), and indoleamine 2,3-dioxygenase (IDO), increased along with immune cell densities in the relapse biopsy (Figure S7E). Increased expression of genes associated with Th1 and NK cell activation and cytotoxicity,

along with increased TIL and NK cell infiltration observed in the relapse biopsy, may be signs of immunologic activation induced by nanril monotherapy and are consistent with the partial clinical response. However, an increase in PD-L1 and Treg densities together with a substantial activation of several immunological checkpoints most likely indicates the development of acquired adaptive immune resistance to nanril monotherapy as evidenced by clinical progression.

Five other patients from the monotherapy part (19.2%) had stable disease (SD). In the combination part (n = 19), a complete response (CR) was observed in 1 patient (5.3%) with mesothelioma (Figure 4C). Three patients (15.8%; thyroid carcinoma, skin melanoma, and cervical melanoma) achieved PR; 2 of these patients (skin melanoma and cervical melanoma) were pre-treated with an ICB. Ten patients (52.6%) had SD, which was maintained



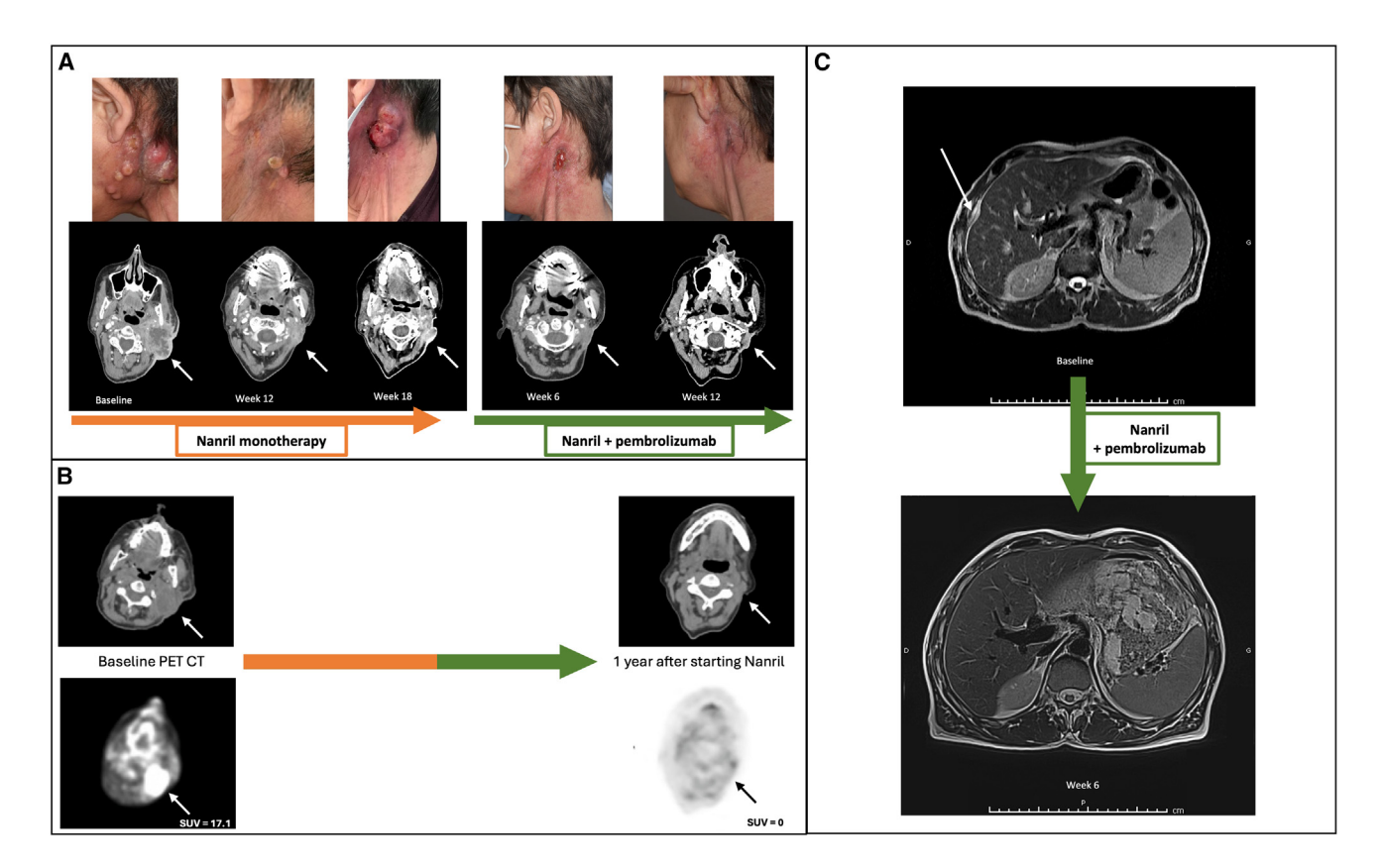


Figure 4. Example of responses observed with nanril as monotherapy or combined with pembrolizumab

(A and B) Confirmed partial response after treatment with nanril as monotherapy and combined with pembrolizumab. A patient with skin squamous cell carcinoma, previously refractory to the immune checkpoint blocker cemiplimab (anti-PD-1), was treated with nanril at 6 μg/kg and achieved confirmed PR. After relapse, the patient crossed over to the combination part of the trial (nanril 1.5 μg/kg in combination with pembrolizumab) and again developed a confirmed and durable clinical benefit. (A) Clinical and radiological evolution over time. (B) Positron emission tomography/computed tomography (PET/CT) imaging at baseline and 1 year later.

(C) Complete response observed in a patient with mesothelioma with nanril as combined with pembrolizumab. Baseline and on-treatment (week 6) MRI scans showing CR in a patient with mesothelioma. The arrow indicates the target lesion (perihepatic peritoneal nodule). See also Figure S7.

for more than 40 weeks in 1 patient with anal squamous cell carcinoma (Figure 3; Table 2). The median progression-free survival was 1.6 months (95% confidence interval [CI] 1.2–2.6) in the monotherapy part and 4.6 months (95% CI 2.5–12.5) in the combination part. The median overall survival was 15.2 months (95% CI 7.6–not reached [NR]) in the monotherapy part and NR in the combination part (95% CI 9.7–NR; Table 2). At 6 months of treatment, a durable clinical benefit was observed in 6 patients in the combination part: 4 patients had ongoing SD and 2 had long-lasting PR.

No pseudoprogression was observed in the monotherapy part. The patient who crossed over to the combination part after relapse in the monotherapy part achieved PR, and one patient in the combination part had SD after unconfirmed disease progression.

Focusing on clinically relevant (biologically active) dose levels of 6–12  $\mu$ g/kg nanril only (n = 12), 1 patient had PR (ORR = 8.3%) and 5 patients had SD (DCR = 50%) in the monotherapy part. In the corresponding dose groups of the combination part (n = 13), 1 patient achieved CR, 2 had PR (ORR = 23%), and 8 had SD (DCR = 85%) as the best response.

### Immune stimulatory properties of nanril in blood and tumors from treated cancer patients

In peripheral blood, nanril monotherapy (27 patients; Figures 5A-5C and S8A) or combined with pembrolizumab (21 patients; Figures 5D-5F and S8C) increased PD markers associated with the expected mode of action of nanril, including proliferating (Ki67+) NK cells, NKT cells, total and effector memory CD8+ T cells and CD4+ T cells (Figures 5A-5D), absolute counts of NK cells, total and effector memory CD8+ T cells (Figures 5B-5E), activation (NKG2D+) of NK cells and total and effector memory CD8+ T cells (Figures S8A and S8C), and interferon (IFN)-γ levels (Figures 5C–5F). Strong proliferation of NK cells was apparent at 0.25 µg/kg, while the activation of CD8+ T cells, memory CD8+ T cells, and NKT cells was dose dependent, reaching a plateau at 12 µg/kg. The slight proliferation of Tregs (Figures 5A-5D) did not translate into significantly increased numbers of Tregs (Figures 5B-5E) or percentages of Tregs in CD4<sup>+</sup> T cells (Figures S8A and S8C).

In tumors, nanril monotherapy increased the density of CD3<sup>+</sup>, CD4<sup>+</sup>, and CD8<sup>+</sup> TILs, the CD8<sup>+</sup>/Treg ratio, and the densities of

#### **Article**



Table 2. Efficacy outcomes		
Variable	Monotherapy	Combination
_	(N = 26)	(N = 19)
Best overall response, n (%)		
CR	0 (0.0)	1 (5.3)
PR	1 (3.8)	3 (15.8)
SD	5 (19.2)	10 (52.6)
UPD	16 (61.5)	2 (10.5)
CPD	3 (11.5)	3 (15.8)
NE	1 (3.8)	0
Overall iRECIST ORR (CR + PR)	3.8%	21.1%
Overall DCR (CR + PR + SD)	23.1%	73.7%
Median PFS, months (95% CI)	1.6 (1.2-2.6)	4.6 (2.5-12.5)
Median duration of response, months (95% CI)	NA	NR (3.9; NR)
Median OS, months (95% CI)	15.2 (7.6-NR)	NR (9.7-NR)
OS at 6 months (%)	83.6	86.9

CI, confidence interval; CPD, confirmed progressive disease; CR, complete response; DCR, disease control rate; NA, not applicable; NE, not evaluable (did not meet the minimum duration criteria to be classified as SD); NR, not reached; ORR, objective response rate; OS, overall survival; PFS, progression-free survival; PR, partial response; SD, stable disease; UPD, unconfirmed progressive disease.

proliferating CD8+ and CD4+ TILs (Figures 5G and S8B). These trends were most apparent in patients with clinical benefit defined as PR or SD (4 out of 5 patients tested). A slight increase in Tregs was observed in patients with clinical benefit, while a slight decrease in Tregs was observed in patients with progressive disease. These effects were not statistically significant, probably due to the small number of patients. Figure S9A shows representative images of immune cells in the tumor from a patient with kidney cancer with SD in the monotherapy part. Consistent with the increased number of TILs, nanril increased the expression of a set of genes associated with effector T cells, Th1, chemokines, and cytokines (Immunosign21)<sup>26</sup> (Figure 5H) and upregulated genes related to the innate and adaptive immune response, including NK cell functions, Th1 activation, regulation of the immune response, chemokines, and  $\gamma\delta$ T cells, primarily in patients with clinical benefit (Figure S10A). In the monotherapy part, no significant differences in PD-L1 density in pretreatment tumor biopsy were observed between patients with clinical benefit and patients with progressive disease

Interestingly, combination treatment led to increased numbers of total and proliferating CD8+ TILs in tumor islets, increased CD8+/Treg ratio in tumor islets, and enhanced clustering of CD8+ TILs in the whole tumor. Recruitment of NK cells into the tumor stroma and islets was observed. These trends were more pronounced in patients with clinical benefit (Figures 5I and S8D). Figure S9B shows representative images of immune cells in the tumor of a patient with cervical cancer with clinical benefit of combination therapy. The expression of Immunosign21 genes (Figure 5J) and genes related to NK cell functions, Th1 activation,  $\gamma\delta$  T cells, and regulation of immune responses (Figures 5J and S10B) was enhanced in tumors, consistent

with the findings for nanril monotherapy. In the combination part, a trend for increased PD-L1 expression in pretreatment tumor biopsies was observed in patients with clinical benefit compared to patients with progressive disease. However, the data are limited by the small number of samples (Figure S8D).

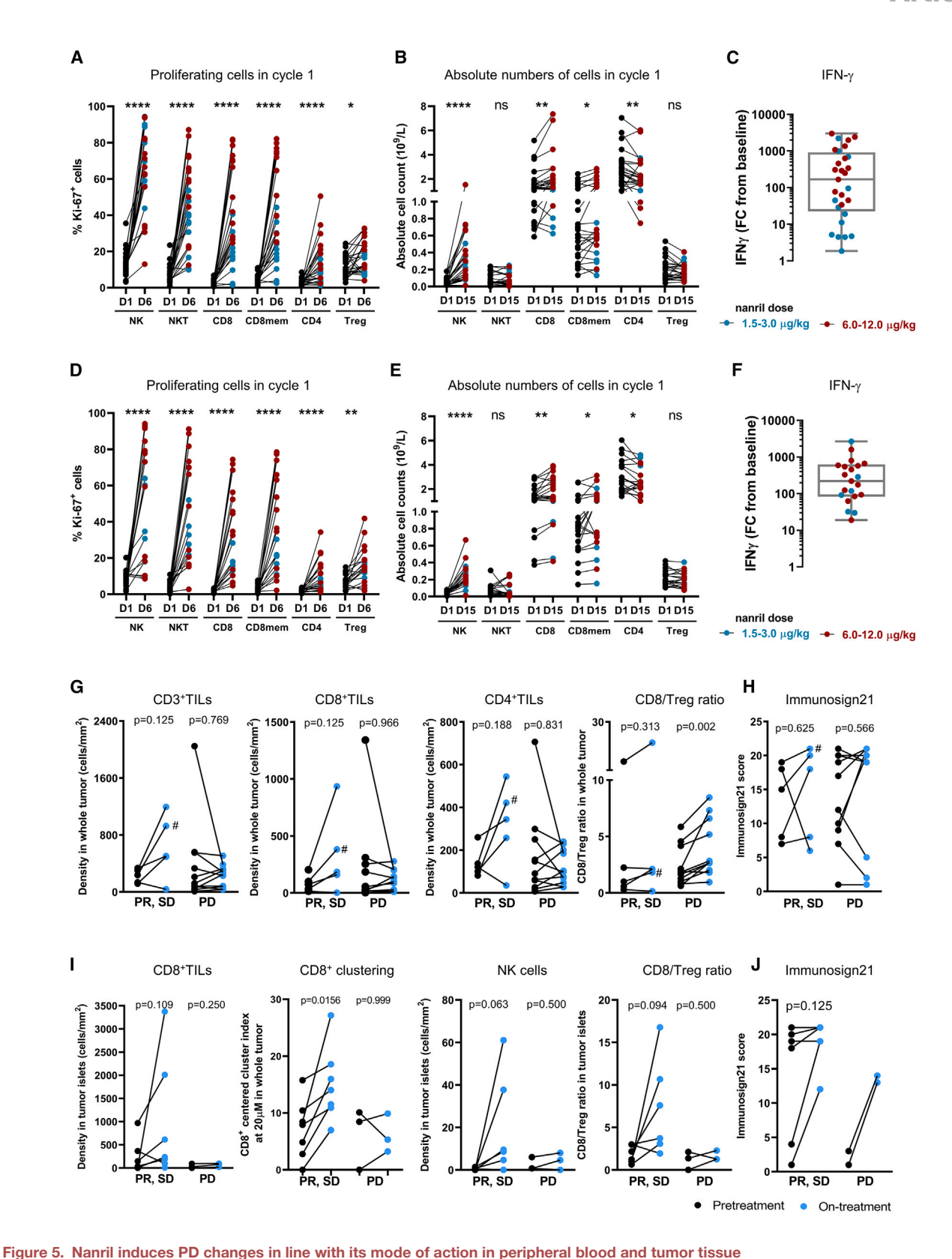
#### **DISCUSSION**

Here, we investigated nanril, a next-generation IL-15 immunotherapy designed to enhance anti-tumor responses, as monotherapy and/or combined with pembrolizumab. The non-clinical studies demonstrated that nanril monotherapy engaged NK and CD8+ T cells to stimulate an inflammatory tumor microenvironment and effective anti-tumor efficacy. This effect was especially evident when combining nanril with an anti-PD-1 antibody in murine models. By documenting the important role of NK cells in the anti-tumor efficacy of nanril as monotherapy and combined with an anti-PD-1 antibody, we have extended previous observations in strictly T cell-dependent murine models. 16 Our data also suggest the potential involvement of other targeted immune cell populations, such as NKT or  $\gamma\delta$  T cells,<sup>27</sup> because depletion of NK and CD8<sup>+</sup> T cells did not completely abolish the anti-tumor activity of nanril combined with an anti-PD-1 antibody.

NK cells play pivotal roles in T cell-dependent and T cell-independent tumor control, thereby contributing to ICB responses.<sup>28</sup> The early intratumoral accumulation of IFN-γ-producing NK cells, besides direct tumor cell killing, can induce tumor microenvironment remodeling and cytotoxic T cell-mediated tumor eradication. Continuous exposure of NK cells to IL-15 induced high NK cell numbers, although it led to functional exhaustion of NK cells.<sup>29,30</sup> A cycle-dependent decrease in the proliferation and high numbers of NK cells were observed in cynomolgus monkeys administered nanril s.c. weekly for 10 weeks. Introducing a 1- or 2-week off-treatment period to the 21-day cycle and repetitive stimulation (days 1, 2, 8, and 9) reactivated the NK cells without decreasing their proliferative capacity, while retaining high CD8<sup>+</sup> T cell activity. This is consistent with the discontinuity theory of immunity in which the innate and adaptive immune systems respond to sudden changes in stimulation and are rendered tolerant by slow or continuous stimulation. 31 The correlation of PD, cell activity, and functionality<sup>18</sup> between humans and cynomolgus monkeys rationalized the dosing regimen used in the phase 1/1b clinical trial.

Nanril was well tolerated as monotherapy and combined with the PD-1 blocker pembrolizumab without relevant overlapping toxicities in 51 heavily pre-treated patients with advanced/metastatic solid tumors. No treatment-related deaths occurred, and most TEAEs were mild. Asymptomatic lymphopenia, the most frequent grade >2 TEAE, may be connected to the mode of action of nanril, involving lymphocyte migration from the periphery to tissues, as reported for IL-15 in cynomolgus monkeys. Nevertheless, the overall safety profile of nanril is comparable to that of other s.c. IL-15 investigational drugs that have been evaluated in studies in human solid tumors, in which transient pyrexia and injection site reactions were common side effects. 5,6,33 Of note, no nanril-related cardiac toxicity or capillary leak syndrome was reported.





PD in peripheral blood during cycle 1 and in paired tumor tissues prior to and during therapy in patients treated with nanril as monotherapy (A–C, G and H) or in combination with pembrolizumab (D–F, I and J). (A, B D, and E) (A, D) The percentage of proliferating (Ki67<sup>+</sup>) and (B, E) absolute numbers of NK, NKT, CD8<sup>+</sup>T cells,

(legend continued on next page)

#### **Article**



We also obtained encouraging efficacy results for nanril, with confirmed CR in 1 patient and confirmed PR in 3 patients. The patient with CR and 1 patient with PR in the combination part were ICB naive, so we cannot distinguish the effect of nanril from that of pembrolizumab. However, two patients with PR were pre-treated with an ICB. One was a patient with sSCC initially refractory to anti-PD-1 therapy (cemiplimab). She had a complete metabolic response in the combination part for over 2 years, indicating that nanril can overcome resistance and synergize with anti-PD-1 therapy.

For sSCC, the current frontline standard of care is ICB therapy.<sup>34</sup> The median duration of response observed in patients with metastatic disease treated with ICBs was longer than 12 months,<sup>35–37</sup> but unlike the patient with durable PR in our study, these patients were ICB naive. Patients who are ineligible for ICBs or who progress on ICBs should be treated with platinum-based chemotherapy with or without cetuximab or epidermal growth factor receptor antibodies.<sup>34</sup> The responses observed with cetuximab monotherapy<sup>38</sup> and cetuximab in combination with pembrolizumab after initial failure<sup>39</sup> lasted more than 20 months, which is similar to the long-lasting PR observed in our study.

The first IL-15 molecule approved by the Food and Drug Administration was N-803 (ALT-803) on April 22, 2024. Despite a similar mechanism of action, there are important differences between nanril and N-803. In nanril, IL-15 is covalently bound to the sushi+ domain of IL-15Rα, whereas in N-803, IL-15 (N72A mutant) is non-covalently complexed to the sushi+ domain of IL-15Ra, and the molecule also contains an Fc-part of an IgG1 antibody. The non-covalent nature of the IL-15/IL-15Rα sushi complex in N-803 allows for dissociation and release of IL-15, which may contribute to the observed clinical safety profile of N-803, together with the Fc-mediated binding to immune cells. In addition, N-803 has a longer half-life due to the presence of the Fc-part of the molecule. This is reflected in the different dosing intervals of the two drugs. It has been shown that prolonged activation of NK cells leads to their unresponsiveness and exhaustion.<sup>29</sup> The experimentally selected nanril dosing is well balanced for optimal activation of both NK and CD8+ T cells. Dissociated IL-15, together with the binding of N-803 to Fc gamma receptors, may contribute to some of the toxicities reported in the N-803 clinical trials.

The changes in peripheral PD observed in patients support the mode of action of nanril. As expected from the non-clinical findings and previous data, <sup>14–18</sup> nanril increased the proliferation of CD8<sup>+</sup> T cells, memory CD8<sup>+</sup> T cells, NK cells, and NKT cells; absolute NK and CD8<sup>+</sup> and memory CD8<sup>+</sup> T cell counts; as well as

IFN-γ levels without concomitantly increasing Tregs. The maximum PD activity of nanril in terms of cell proliferation was reached at 12 µg/kg, corresponding to the maximum PD activity observed in vitro and in vivo in cynomolgus monkeys. Blood PD activity of nanril was observed in all patients, regardless of their clinical response, with dose-dependent activation of CD8+ T cells and increased IFN- $\gamma$  production at 6, 9, and 12  $\mu g/kg$ . These findings can be correlated with the greater response rate for nanril monotherapy at 6 µg/kg and higher. Importantly, nanril monotherapy increased the density of TILs and activated genes related to innate and adaptive immunity in tumors in 4 of 5 patients with clinical benefit. We also observed trends toward an increased CD8<sup>+</sup>/Treg ratio and increased infiltration of tumor parenchyma with total and proliferating CD8+ T cells and NK cells in patients with clinical benefit after treatment with nanril and pembrolizumab. The observed increase in the CD8/Treg ratio in non-responders appears to be primarily due to a non-significant trend toward a decrease in Tregs after treatment rather than an increase in CD8<sup>+</sup> T cells alone. This observation warrants further investigation. Overall, the immunological changes tended to be less frequent and less pronounced in patients with progressive disease. Immune cell infiltration within the tumor, an increased CD8+T cell/Treg ratio, and mobilization of proliferating CD8<sup>+</sup> T cells toward the tumor parenchyma were shown to be good predictors of the response to immunotherapy. 40-44

In conclusion, nanril as monotherapy and combined with pembrolizumab had a favorable safety profile and conferred clinical benefits in patients with various tumor types, including those who had previously progressed on ICBs. Although the immunological changes in the patients' blood and tumors were consistent with the expected mode of action, further clinical trials are needed to determine whether these changes are reliable predictors of patients' clinical outcome. Our non-clinical and initial clinical experience thus far suggests that nanril activates the immune system and induces inflammatory changes in the tumor microenvironment to exert single-agent activity against certain tumor types or to potentially augment the effects of other immunotherapies. Extended evaluation of nanril combined with pembrolizumab and cetuximab is currently underway in phase 2 clinical trials in patients with selected advanced solid tumors (NCT05256381, NCT05619172).

#### Limitations of the study

There are some limitations to our study. The preclinical species, such as mice and cynomolgus monkeys, may not accurately represent the complexity of human responses, as exemplified by a higher repetitive dosing schedule of nanril in mice

memory CD8<sup>+</sup> T cells, CD4<sup>+</sup> T cells, and Tregs were evaluated by flow cytometry using peripheral blood samples collected pre-dose and at 6 days (Ki67<sup>+</sup>) or 15 days (absolute count) after starting treatment.

See also Figures S8, S9, and S10.

<sup>(</sup>C and F) Maximal fold change in peripheral blood IFN-γ concentrations from baseline. Boxplots show the lower quartile, median, and upper quartile; whiskers represent the minimum and maximum values.

<sup>(</sup>G–J) (G and I) Immune cell infiltration and (H, J) Immunosign21 gene score evaluated using paired tumor biopsies for 16 patients in the monotherapy part and 10 patients in the combination part. Biopsies were collected before treatment and on-treatment (cycle 2 or in week 20) and subjected to immunohistochemistry and NanoString gene analysis. Patients were divided into two groups according to their clinical response. Group 1 includes patients with confirmed PR (labeled #) or SD. Group 2 includes patients with progressive disease (unconfirmed and confirmed).

<sup>\*</sup>p < 0.05, \*\*p < 0.01, \*\*\*p < 0.001, and \*\*\*\*p < 0.0001 (Wilcoxon-Mann-Whitney test). ns, not significant; PR, partial response; SD, stable disease; PD, progressive disease.



to achieve optimal NK and CD8<sup>+</sup> T cell responses, which results from a lower IL-15R sequence identity between mouse and human. Although the evaluation of overall response and the relevant quantitative assessments in the phase 1/1b clinical study of nanril were based on the widely accepted iRE-CIST response criteria, the study was designed as a dose-escalation safety study, and the initial cohorts were treated with sub-therapeutic dose levels of nanril. In addition, the study did not include a control arm or sample size calculations for efficacy evaluations.

#### **RESOURCE AVAILABILITY**

#### Lead contact

Further information and requests for resources and reagents should be directed to and will be fulfilled by the lead contact, Stephane Champiat (schampiat@mdanderson.org).

#### **Materials availability**

This study did not generate new unique reagents.

#### Data and code availability

- The preclinical raw datasets generated and/or analyzed during the current study are not publicly available but may be made available upon reasonable request. Clinical trial data will be made available upon reasonable request to qualified investigators for use in rigorous, independent scientific research, as long as the trials are not part of an ongoing or planned regulatory submission. Data sharing is subject to protection of patient privacy and respect of the patient's informed consent. Data will be made available following review and approval of a research proposal and statistical analysis plan and execution of a data sharing agreement. For approved requests, the data will be available for 12 months, with possible extensions considered. For more information on the process, or to submit a request, please contact the lead contact.
- This paper does not report original code.
- Any additional information required to reanalyze the data reported in this
  paper is available from the lead contact upon request.

#### **ACKNOWLEDGMENTS**

We thank the patients, their families, the investigators, the clinical research staff, and the members of the dose-escalation committee and independent advisory panel for participating in this study. We also thank Lenka Kasikova, Olena Sapega, and Renata Tureckova for technical support during the nonclinical studies and data preparation, Christoph Rehfuess for critically reviewing the results and contribution to scientific discussions, Pavla Kadlecova for statistical support and review of the clinical data analysis, Gabriella Lukacs for data management support, and Ondrej Smid and Nicholas D. Smith for medical writing support.

This study was funded by SOTIO Biotech AG.

#### **AUTHOR CONTRIBUTIONS**

Conceptualization, A.M., D.B., I.A., L.P.J., P.L., R. Spisek, S.C., and U.M.; methodology, A.M., I.A., L.P.J., M.R., N.P., R.M., and R. Spisek.; investigation, A.M., A.N., A.S., C.G.-R., E.G., I.A., I.K., J.K.-K., K.O., L.P.J., N.P., P.A.C., P.G., P.L., R.M., S.C., S.T., and V.G.; visualization, A.S., I.A., and L.P.J.; project administration, I.A., L.P.J., and U.M.; supervision, A.M., D.B., I.A., L.P.J., R. Sachse, R. Spisek, S.C., and U.M.; writing – original draft, A.M., A.S., I.A., J.K.-K., L.P.J., S.C., and S.T.; writing – review and editing, A.M., A.N., A.S., C.G.-R., D.B., E.G., I.A., I.K., J.K.-K., K.O., L.P.J., P.A.C., P.G., P.L., R. Sachse, R. Spisek, S.C., S.T., U.M., and V.G.

#### **DECLARATION OF INTERESTS**

S.C. reports personal fees from AbbVie, Adaptimmune, Adlai Nortye USA Inc., Aduro Biotech, Agios Pharmaceuticals, Alderaan Biotechnology, Amgen, Astellas, Astex Pharmaceuticals, AstraZeneca Ab, AstraZeneca, Avacta, Aveo, Basilea Pharmaceutica International Ltd., Bayer Healthcare Ag, BBB Technologies Bv, BeiGene, BicycleTx Ltd., Blueprint Medicines, Boehringer Ingelheim, Boston Pharmaceuticals, Bristol-Myers Squibb Ca, Casi Pharmaceuticals Inc., Celanese, Celgene Corporation, Cellcentric, Chugai Pharmaceutical Co., Cullinan-Apollo, CureVac, Cytovation, Daiichi Sankyo, Debiopharm, Domain Therapeutics, Eisai, Eisai Limited, Eli Lilly, Ellipses Pharma, Exelixis, Faron Pharmaceuticals Ltd., Forma Therapeutics, GamaMabs, Genentech, Genmab, Genomics, GlaxoSmithKline, H3 Biomedicine, Hoffmann La Roche Ag, ImCheck Therapeutics, Immunicom Inc., Incyte Corporation, Innate Pharma, Institut De Recherche Pierre Fabre, Iris Servier, iTeos Belgium SA, Janssen, Janssen Cilag, Janssen R&D LLC, Janssen Research Foundation, Kura Oncology, Kyowa Kirin Pharm. Dev, Lilly France, Loxo Oncology, Medimmune, Menarini Ricerche, Merck, Merck Serono, Merck, Sharp & Dohme Chibret, OSE Pharma, Merrimack Pharmaceuticals, Merus, Molecular Partners Ag, Nanobiotix, Nektar Therapeutics, Novartis, Novartis Pharma, Octimet Oncology Nv, OncoEthix, Oncopeptides, Oncovita, Orion Pharma, OSE Pharma, Pfizer, PharmaMar, Pierre Fabre, Pierre Fabre Medicament, Relay Therapeutics Inc., Roche, Sanofi Aventis, Seagen, Seattle Genetics, SOTIO Biotech A.S., Syros Pharmaceuticals, Taiho Pharma, Tatum Bioscience, Tesaro, Tollys SAS, Transgene, Transgene S.A, Turning Point Therapeutics, Ultrahuman8, and Xencor; grants from AstraZeneca, Bristol Myers Squibb, Boehringer Ingelheim, GSK, INCA, Janssen Cilag, Merck, Pfizer, Roche, and Sanofi; and non-financial support (drug supplied) from AstraZeneca, Bristol Myers Squibb, Boehringer Ingelheim, GSK, Medimmune, Merck, NH TherAguix, Pfizer, and Roche.

E.G. reports personal fees from Agios Pharmaceuticals, Alkermes, Amgen, Anaveon, Bayer, BeiGene USA, Blueprint Medicines, Boehringer Ingelheim, Bristol Myers Squibb, Cellestia Biotech, Debiopharm, Ellipses Pharma, F. Hoffmann La Roche Ltd., Forma Therapeutics, F-Star Therapeutics, Genentech Inc., Genmab B.V., Glycotope GmbH, GSK, Hengrui, ICO, Incyte Biosciences, Incyte Corporation, Janssen Global Services, Kura Oncology Inc., Lilly, Lilly S.A., Loxo Oncology Inc., MAB Discovery, Macrogenics Inc., Menarini Ricerche Spa, Merck, Sharp & Dohme, Merck, Sharp & Dohme de Espana, S.A, Nanobiotix, S.A, Neomed Therapeutics 1 Inc., Novartis, Novartis Farmaceutica, S.A, Pfizer, SLU, PharmaMar, S.A.U, Pierre Fabre Medicament, Principia Biopharma Inc., PsiOxus Therapeutics Ltd., Roche, Roche/Genentech, Sanofi, Sierra Oncology, Inc., Seagen, SOTIO Biotech A.S., Symphogen A/S, TFS, Thermo Fisher and grants from AstraZeneca, BeiGene, Novartis, Roche, Taiho, and Thermo Fisher outside the submitted work.

V.G. reports institutional support from Affimed GmbH, Anaveon AG, BicycleTx Ltd, BioNTech SE, Boehringer Ingelheim, Celgene Corporation, Debiopharm International S.A., Epizyme Inc., F. Hoffmann-La Roche Ltd., F-star Therapeutics Limited, Genmab, ImCheck Therapeutics, Janssen Research & Development LLC, Novartis, Pieris Pharmaceuticals Inc., Regeneron Pharmaceuticals Inc., Seagen Inc., Shattuck Labs Inc., SOTIO Biotech AG, and T-knife GmbH

P.A.C. has received personal fees from Amgen, Bristol Myers Squibb, Boehringer Ingelheim, Janssen Oncology, OSE Immunotherapeutics, and Roche.

C.G.-R. reports personal fees from Bristol Myers Squibb, Eisai, Foundation Medicine, Macomics, Pierre Fabre, and Roche/Genentech.

P.G. reports consulting or advisory fees and travel expenses from Servier and consulting or advisory fees from Roche outside the submitted work.

A.N. reports personal fees from AbbVie, AKH Inc., Alfaisal University, ARMO BioSciences, ASCO Direct Oncology Highlights, CME Outfitters, CytomX Therapeutics, Deka Biosciences, European Society for Medical Oncology, Genome & Company, Horizon Therapeutics USA Inc., Immune-Onc Therapeutics, Korean Society of Medical Oncology, Lynx Health, Merck Sharp & Dohme Corp., NeoImmuneTech, NGM Bio, Nouscom, OncoNano, OncoSec KEY-NOTE-695, Pharming Healthcare Inc., PsiOxus Therapeutics, Scripps Cancer Care Symposium, Servier, Society for Immunotherapy of Cancer, STCube Pharmaceuticals, Takeda, and The Lynx Group and grants from Amplimmune, Arcus Biosciences, ARMO BioSciences, Atterocor/Millendo, Baxalta US Inc.,

#### **Article**



BioNTech SE, Bristol Myers Squibb, Calithera Biosciences, Chao Physician-Scientist Foundation, CytomX Therapeutics, Eli Lilly, EMD Serono, Healios Onc. Nutrition, Immune Deficiency Foundation, Immune-Onc Therapeutics, Incyte, Jeffery Modell Foundation, Karyopharm Therapeutics, Kymab, Medlmmune, Merck, Monopteros Therapeutics, NCI, NeolmmuneTech, Neon Therapeutics, Novartis, Pfizer, PsiOxus, Regeneron, Seven & Eight Biopharma, SOTIO Biotech AG, Surface Oncology, The Texas Medical Center Digestive Diseases Center, and TopAlliance Biosciences outside the submitted work

P.L. reports personal fees from AbbVie, ABL Bio, Agenus, Agios, Astellas, AstraZeneca, BAKX Therapeutics, Bayer, Black Diamond, Compass BADX, Cybrexa, CytomX, EMD Serono, Five Prime, Genentech, Genmab, Glaxo-Smith Kline, Halozyme, I-Mab, imCheck, ImmunoMet, IQVIA, Kineta Inc., Kyowa Kirin Pharmaceutical Development, MacroGenics, Mekanist, Mersana Therapeutics, Molecular Templates, NeuroTrials, Pfizer, QED Therapeutics, Qualigen, Relay Therapeutics, Roche/Genentech, Roivant Sciences, Salarius, Scenic Biotech, Seagen, Shattuck, Silverback, SK Life Science, SOTIO Biotech A.S., STCube Pharmaceuticals, Stemline, Takeda, TRIGR, Tyme, and Zentalis Pharmaceuticals.

R.M. reports support from SOTIO Biotech A.S.

N.P. is an employee of SOTIO Biotech A.S. and reports international patents/patent applications (WO 2020/234387, WO 2022/090202, and WO 2022/090203) with Cytune Pharma.

M.R. reports support from SOTIO Biotech A.S.

A.S. is an employee of SOTIO Biotech A.S.

J.K.-K. is an employee of SOTIO Biotech AG.

S.T. is an employee of SOTIO Biotech AG.

R. Sachse is an employee of SOTIO Biotech AG.

U.M. is an employee of SOTIO Biotech A.S. and reports the following international patents/patent applications (WO 2020/234387, WO 2022/090202, WO 2022/090203, PCT/EP2022/067253, PCT/EP2022/067236, and PCT/EP2022/072845) with Cytune Pharma.

R. Spisek is an employee of SOTIO Biotech A.S.

D.B. reports international patents/patent applications (WO 2012/175222, WO 2014/170032, WO 2015/018528, WO 2015/131994, WO 2015/018529, WO 2020/234387, WO 2022/090202, WO 2022/090203, PCT/EP2022/067253, PCT/EP2022/067236, and PCT/EP2022/072845) with Cytune Pharma.

L.P.G. is an employee of SOTIO Biotech A.S.

I.A. is an employee of SOTIO Biotech A.S. and reports international patents/patent applications (WO 2020/234387, WO 2022/090202, WO 2022/090203, PCT/EP2022/067253, PCT/EP2022/067236, and PCT/EP2022/072845) with Cvtune Pharma.

A.M. was the principal investigator for the AURELIO-03 (ClinicalTrials.gov identifier: NCT04234113) trial of nanril. He was compensated for providing expertise to SOTIO Biotech AG and Cytune Pharma through scientific advisory boards and consulting time. He received expense reimbursements for travel and housing and fees for presenting nanril data at international scientific meetings. He is currently part of the scientific advisory board of other companies developing immunocytokines: Deka Biosciences and Marengo Therapeutics.

#### **STAR**\***METHODS**

Detailed methods are provided in the online version of this paper and include the following:

- KEY RESOURCES TABLE
- EXPERIMENTAL MODEL AND STUDY PARTICIPANT DETAILS
  - Cell culture and cell lines
  - o In vivo animal studies
- METHOD DETAILS
  - Reagents and antibodies
  - Non-clinical anti-tumor efficacy studies
  - $_{\odot}\,$  Immunophenotyping and gene expression in mice
  - $_{\odot}\,$  In vitro potency assays of human PBMCs
  - $\,\circ\,$  Flow cytometry of human and mouse samples
  - Cynomolgus monkey studies

- Clinical trial
- Translational analyses
- QUANTIFICATION AND STATISTICAL ANALYSIS
  - Sample size
  - Analysis sets
  - Statistical analyses
- ADDITIONAL RESOURCES

#### SUPPLEMENTAL INFORMATION

Supplemental information can be found online at https://doi.org/10.1016/j.xcrm.2025.101967.

Received: January 18, 2024 Revised: October 15, 2024 Accepted: January 16, 2025 Published: February 10, 2025

#### REFERENCES

- Cheever, M.A. (2008). Twelve immunotherapy drugs that could cure cancers. Immunol. Rev. 222, 357–368. https://doi.org/10.1111/j.1600-065X. 2008 00604 x
- Dutcher, J.P., Schwartzentruber, D.J., Kaufman, H.L., Agarwala, S.S., Tarhini, A.A., Lowder, J.N., and Atkins, M.B. (2014). High dose interleukin-2 (Aldesleukin) expert consensus on best management practices-2014.
   J. Immunother. Cancer 2, 26. https://doi.org/10.1186/s40425-014-0026-0
- 3. Rosenberg, S.A. (2014). IL-2: the first effective immunotherapy for human cancer. J. Immunol. *192*, 5451–5458. https://doi.org/10.4049/jimmunol. 1400019
- Conlon, K.C., Lugli, E., Welles, H.C., Rosenberg, S.A., Fojo, A.T., Morris, J.C., Fleisher, T.A., Dubois, S.P., Perera, L.P., Stewart, D.M., et al. (2015). Redistribution, hyperproliferation, activation of natural killer cells and CD8 T cells, and cytokine production during first-in-human clinical trial of recombinant human interleukin-15 in patients with cancer. J. Clin. Oncol. 33, 74–82. https://doi.org/10.1200/JCO.2014.57.3329.
- Miller, J.S., Morishima, C., McNeel, D.G., Patel, M.R., Kohrt, H.E.K., Thompson, J.A., Sondel, P.M., Wakelee, H.A., Disis, M.L., Kaiser, J.C., et al. (2018). A first-in-human phase I study of subcutaneous outpatient recombinant human IL15 (rhlL15) in adults with advanced solid tumors. Clin. Cancer Res. 24, 1525–1535. https://doi.org/10.1158/1078-0432.CCR-17-2451
- Margolin, K., Morishima, C., Velcheti, V., Miller, J.S., Lee, S.M., Silk, A.W., Holtan, S.G., Lacroix, A.M., Fling, S.P., Kaiser, J.C., et al. (2018). Phase I trial of ALT-803, a novel recombinant IL15 complex, in patients with advanced solid tumors. Clin. Cancer Res. 24, 5552–5561. https://doi. org/10.1158/1078-0432.CCR-18-0945.
- Fiore, P.F., Di Matteo, S., Tumino, N., Mariotti, F.R., Pietra, G., Ottonello, S., Negrini, S., Bottazzi, B., Moretta, L., Mortier, E., and Azzarone, B. (2020). Interleukin-15 and cancer: some solved and many unsolved questions. J. Immunother. Cancer 8, e001428. https://doi.org/10.1136/jitc-2020-001428.
- 8. Waldmann, T.A., Dubois, S., Miljkovic, M.D., and Conlon, K.C. (2020). IL-15 in the combination immunotherapy of cancer. Front. Immunol. *11*, 868. https://doi.org/10.3389/fimmu.2020.00868.
- Zhang, X., Sun, S., Hwang, I., Tough, D.F., and Sprent, J. (1998). Potent and selective stimulation of memory-phenotype CD8+ T cells in vivo by IL-15. Immunity 8, 591–599. https://doi.org/10.1016/s1074-7613(00) 80564-6.
- Marks-Konczalik, J., Dubois, S., Losi, J.M., Sabzevari, H., Yamada, N., Feigenbaum, L., Waldmann, T.A., and Tagaya, Y. (2000). IL-2-induced activation-induced cell death is inhibited in IL-15 transgenic mice. Proc. Natl. Acad. Sci. USA 97, 11445–11450. https://doi.org/10.1073/pnas. 200363097.



- Waldmann, T.A. (2015). The shared and contrasting roles of IL2 and IL15 in the life and death of normal and neoplastic lymphocytes: implications for cancer therapy. Cancer Immunol. Res. 3, 219–227. https://doi.org/10. 1158/2326-6066.CIR-15-0009.
- Mortier, E., Quéméner, A., Vusio, P., Lorenzen, I., Boublik, Y., Grötzinger, J., Plet, A., and Jacques, Y. (2006). Soluble interleukin-15 receptor alpha (IL-15R alpha)-sushi as a selective and potent agonist of IL-15 action through IL-15R beta/gamma. Hyperagonist IL-15 x IL-15R alpha fusion proteins. J. Biol. Chem. 281, 1612–1619. https://doi.org/10.1074/jbc. M508624200.
- Bouchaud, G., Garrigue-Antar, L., Solé, V., Quéméner, A., Boublik, Y., Mortier, E., Perdreau, H., Jacques, Y., and Plet, A. (2008). The exon-3-encoded domain of IL-15ralpha contributes to IL-15 high-affinity binding and is crucial for the IL-15 antagonistic effect of soluble IL-15Ralpha. J. Mol. Biol. 382, 1–12. https://doi.org/10.1016/j.jmb.2008.07.019.
- Huntington, N.D., Legrand, N., Alves, N.L., Jaron, B., Weijer, K., Plet, A., Corcuff, E., Mortier, E., Jacques, Y., Spits, H., and Di Santo, J.P. (2009). IL-15 trans-presentation promotes human NK cell development and differentiation in vivo. J. Exp. Med. 206, 25–34. https://doi.org/10.1084/jem. 20082013.
- Huntington, N.D., Alves, N.L., Legrand, N., Lim, A., Strick-Marchand, H., Mention, J.J., Plet, A., Weijer, K., Jacques, Y., Becker, P.D., et al. (2011). IL-15 transpresentation promotes both human T-cell reconstitution and T-cell-dependent antibody responses in vivo. Proc. Natl. Acad. Sci. USA 108, 6217–6222. https://doi.org/10.1073/pnas.1019167108.
- Desbois, M., Le Vu, P., Coutzac, C., Marcheteau, E., Béal, C., Terme, M., Gey, A., Morisseau, S., Teppaz, G., Boselli, L., et al. (2016). IL-15 transsignaling with the superagonist RLI promotes effector/memory CD8+ T cell responses and enhances antitumor activity of PD-1 antagonists. J. Immunol. 197, 168-178. https://doi.org/10.4049/jimmunol.1600019.
- Desbois, M., Béal, C., Charrier, M., Besse, B., Meurice, G., Cagnard, N., Jacques, Y., Béchard, D., Cassard, L., and Chaput, N. (2020). IL-15 superagonist RLI has potent immunostimulatory properties on NK cells: implications for antimetastatic treatment. J. Immunother. Cancer 8, e000632. https://doi.org/10.1136/jitc-2020-000632.
- Antosova, Z., Podzimkova, N., Tomala, J., Augustynkova, K., Sajnerova, K., Nedvedova, E., Sirova, M., de Martynoff, G., Bechard, D., Moebius, U., et al. (2022). SOT101 induces NK cell cytotoxicity and potentiates antibody-dependent cell cytotoxicity and anti-tumor activity. Front. Immunol. 13, 989895. https://doi.org/10.3389/fimmu.2022.989895.
- Bessard, A., Solé, V., Bouchaud, G., Quéméner, A., and Jacques, Y. (2009). High antitumor activity of RLI, an interleukin-15 (IL-15)-IL-15 receptor alpha fusion protein, in metastatic melanoma and colorectal cancer. Mol. Cancer Therapeut. 8, 2736–2745. https://doi.org/10.1158/1535-7163 MCT-09-0275
- Nixon, N.A., Blais, N., Ernst, S., Kollmannsberger, C., Bebb, G., Butler, M., Smylie, M., and Verma, S. (2018). Current landscape of immunotherapy in the treatment of solid tumours, with future opportunities and challenges. Curr. Oncol. 25, e373–e384. https://doi.org/10.3747/co.25.3840.
- Sharma, P., Siddiqui, B.A., Anandhan, S., Yadav, S.S., Subudhi, S.K., Gao, J., Goswami, S., and Allison, J.P. (2021). The next decade of immune checkpoint therapy. Cancer Discov. 11, 838–857. https://doi.org/10. 1158/2159-8290.CD-20-1680.
- Gong, J., Chehrazi-Raffle, A., Reddi, S., and Salgia, R. (2018). Development of PD-1 and PD-L1 inhibitors as a form of cancer immunotherapy: a comprehensive review of registration trials and future considerations.
   J. Immunother. Cancer 6, 8. https://doi.org/10.1186/s40425-018-0316-z.
- Marabelle, A., Le, D.T., Ascierto, P.A., Di Giacomo, A.M., De Jesus-Acosta, A., Delord, J.P., Geva, R., Gottfried, M., Penel, N., Hansen, A.R., et al. (2020). Efficacy of pembrolizumab in patients with noncolorectal high microsatellite instability/mismatch repair-deficient cancer: results from the phase II KEYNOTE-158 study. J. Clin. Oncol. 38, 1–10. https://doi.org/10.1200/JCO.19.02105.

- Dammeijer, F., Lau, S.P., van Eijck, C.H.J., van der Burg, S.H., and Aerts, J.G.J.V. (2017). Rationally combining immunotherapies to improve efficacy of immune checkpoint blockade in solid tumors. Cytokine Growth Factor Rev. 36, 5–15. https://doi.org/10.1016/j.cytogfr.2017.06.011.
- Sun, J.Y., Zhang, D., Wu, S., Xu, M., Zhou, X., Lu, X.J., and Ji, J. (2020).
   Resistance to PD-1/PD-L1 blockade cancer immunotherapy: mechanisms, predictive factors, and future perspectives. Biomark. Res. 8, 35. https://doi.org/10.1186/s40364-020-00212-5.
- Scholler, N., Perbost, R., Locke, F.L., Jain, M.D., Turcan, S., Danan, C., Chang, E.C., Neelapu, S.S., Miklos, D.B., Jacobson, C.A., et al. (2022). Tumor immune contexture is a determinant of anti-CD19 CAR T cell efficacy in large B cell lymphoma. Nat. Med. 28, 1872–1882. https://doi.org/10. 1038/s41591-022-01916-x.
- Guo, Y., Luan, L., Patil, N.K., and Sherwood, E.R. (2017). Immunobiology
  of the IL-15/IL-15Ralpha complex as an antitumor and antiviral agent.
  Cytokine Growth Factor Rev. 38, 10–21. https://doi.org/10.1016/j.cy-togfr.2017.08.002.
- Bonavita, E., Bromley, C.P., Jonsson, G., Pelly, V.S., Sahoo, S., Walwyn-Brown, K., Mensurado, S., Moeini, A., Flanagan, E., Bell, C.R., et al. (2020).
   Antagonistic inflammatory phenotypes dictate tumor fate and response to immune checkpoint blockade. Immunity 53, 1215–1229.e8. https://doi.org/10.1016/j.immuni.2020.10.020.
- Felices, M., Lenvik, A.J., McElmurry, R., Chu, S., Hinderlie, P., Bendzick, L., Geller, M.A., Tolar, J., Blazar, B.R., and Miller, J.S. (2018). Continuous treatment with IL-15 exhausts human NK cells via a metabolic defect. JCI insight 3, e96219. https://doi.org/10.1172/jci.insight.96219.
- Elpek, K.G., Rubinstein, M.P., Bellemare-Pelletier, A., Goldrath, A.W., and Turley, S.J. (2010). Mature natural killer cells with phenotypic and functional alterations accumulate upon sustained stimulation with IL-15/IL-15Ralpha complexes. Proc. Natl. Acad. Sci. USA 107, 21647–21652. https://doi.org/10.1073/pnas.1012128107.
- Pradeu, T., and Vivier, E. (2016). The discontinuity theory of immunity. Sci. Immunol. 1, AAG0479. https://doi.org/10.1126/sciimmunol.aag0479.
- Lugli, E., Goldman, C.K., Perera, L.P., Smedley, J., Pung, R., Yovandich, J.L., Creekmore, S.P., Waldmann, T.A., and Roederer, M. (2010). Transient and persistent effects of IL-15 on lymphocyte homeostasis in nonhuman primates. Blood *116*, 3238–3248. https://doi.org/10.1182/blood-2010-03-275438.
- Conlon, K., Watson, D.C., Waldmann, T.A., Valentin, A., Bergamaschi, C., Felber, B.K., Peer, C.J., Figg, W.D., Potter, E.L., Roederer, M., et al. (2021). Phase I study of single agent NIZ985, a recombinant heterodimeric IL-15 agonist, in adult patients with metastatic or unresectable solid tumors.
   J. Immunother. Cancer 9, e003388. https://doi.org/10.1136/jitc-2021-003388
- 34. National Comprehensive Cancer Network. NCCN Guideline: Squamous cell skin cancer, version 1.2024. https://www.nccn.org/.
- Rischin, D., Khushalani, N.I., Schmults, C.D., Guminski, A., Chang, A.L.S., Lewis, K.D., Lim, A.M., Hernandez-Aya, L., Hughes, B.G.M., Schadendorf, D., et al. (2021). Integrated analysis of a phase 2 study of cemiplimab in advanced cutaneous squamous cell carcinoma: extended follow-up of outcomes and quality of life analysis. J. Immunother. Cancer 9, e002757. https://doi.org/10.1136/jitc-2021-002757.
- Hughes, B.G.M., Munoz-Couselo, E., Mortier, L., Bratland, Å., Gutzmer, R., Roshdy, O., González Mendoza, R., Schachter, J., Arance, A., Grange, F., et al. (2021). Pembrolizumab for locally advanced and recurrent/metastatic cutaneous squamous cell carcinoma (KEYNOTE-629 study): an open-label, nonrandomized, multicenter, phase II trial. Ann. Oncol. 32, 1276–1285. https://doi.org/10.1016/j.annonc.2021.07.008.
- Clingan, P., Ladwa, R., Brungs, D., Harris, D.L., McGrath, M., Arnold, S., Coward, J., Fourie, S., Kurochkin, A., Malan, D.R., et al. (2023). Efficacy and safety of cosibelimab, an anti-PD-L1 antibody, in metastatic cutaneous squamous cell carcinoma. J. Immunother. Cancer 11, e007637. https://doi.org/10.1136/jitc-2023-007637.

#### **Article**



- Marin-Acevedo, J.A., Withycombe, B.M., Kim, Y., Brohl, A.S., Eroglu, Z., Markowitz, J., Tarhini, A.A., Tsai, K.Y., and Khushalani, N.I. (2023). Cetuximab for immunotherapy-refractory/ineligible cutaneous squamous cell carcinoma. Cancers 15, 3180. https://doi.org/10.3390/cancers15123180.
- Bossi, P., Alberti, A., Bergamini, C., Resteghini, C., Locati, L.D., Alfieri, S., Cavalieri, S., Colombo, E., Gurizzan, C., Lorini, L., et al. (2022). Immunotherapy followed by cetuximab in locally advanced/metastatic (LA/M) cutaneous squamous cell carcinomas (cSCC): The I-TACKLE trial. J. Clin. Oncol. 40, 9520. https://doi.org/10.1200/JCO.2022.40. 16 suppl.9520.
- Quezada, S.A., Peggs, K.S., Curran, M.A., and Allison, J.P. (2006). CTLA4 blockade and GM-CSF combination immunotherapy alters the intratumor balance of effector and regulatory T cells. J. Clin. Invest. 116, 1935–1945. https://doi.org/10.1172/JCl27745.
- Fridman, W.H., Pagès, F., Sautès-Fridman, C., and Galon, J. (2012). The immune contexture in human tumours: impact on clinical outcome. Nat. Rev. Cancer 12, 298–306. https://doi.org/10.1038/nrc3245.
- Ye, Y., Zhang, Y., Yang, N., Gao, Q., Ding, X., Kuang, X., Bao, R., Zhang, Z., Sun, C., Zhou, B., et al. (2022). Profiling of immune features to predict immunotherapy efficacy. Innovation 3, 100194. https://doi.org/10.1016/j. xinn.2021.100194.

- Ott, P.A., Hu-Lieskovan, S., Chmielowski, B., Govindan, R., Naing, A., Bhardwaj, N., Margolin, K., Awad, M.M., Hellmann, M.D., Lin, J.J., et al. (2020). A phase lb trial of personalized neoantigen therapy plus anti-PD-1 in patients with advanced melanoma, non-small cell lung cancer, or bladder cancer. Cell 183, 347–362.e24. https://doi.org/10.1016/j.cell. 2020.08.053.
- 44. Tumeh, P.C., Harview, C.L., Yearley, J.H., Shintaku, I.P., Taylor, E.J.M., Robert, L., Chmielowski, B., Spasic, M., Henry, G., Ciobanu, V., et al. (2014). PD-1 blockade induces responses by inhibiting adaptive immune resistance. Nature 515, 568–571. https://doi.org/10.1038/nature13954.
- Foster, B.A., Gingrich, J.R., Kwon, E.D., Madias, C., and Greenberg, N.M. (1997). Characterization of prostatic epithelial cell lines derived from transgenic adenocarcinoma of the mouse prostate (TRAMP) model. Cancer Res. 57, 3325–3330.
- Lin, K.Y., Guarnieri, F.G., Staveley-O'Carroll, K.F., Levitsky, H.I., August, J.T., Pardoll, D.M., and Wu, T.C. (1996). Treatment of established tumors with a novel vaccine that enhances major histocompatibility class II presentation of tumor antigen. Cancer Res. 56, 21–26.
- Le Tourneau, C., Lee, J.J., and Siu, L.L. (2009). Dose escalation methods in phase I cancer clinical trials. J. Natl. Cancer Inst. 101, 708–720. https://doi.org/10.1093/jnci/djp079.



#### **STAR**\***METHODS**

#### **KEY RESOURCES TABLE**

REAGENT or RESOURCE	SOURCE	IDENTIFIER	
Antibodies			
Anti-CD45	BD Biosciences	Cat#561294, RRID:AB_10612014	
Anti-CD3	BD Biosciences	Cat#557757, RRID:AB_396863	
Anti-CD4	BD Biosciences	Cat#560811, RRID:AB_2033927	
Anti-CD8	BD Biosciences	Cat#564116, RRID:AB_2869551	
Anti-Ki67	BD Biosciences	Cat#561277, RRID:AB_10611571	
Anti-CD20	BD Biosciences	Cat#555623, RRID:AB_395989	
anti-CD25	eBioscience	Cat#17-0257-42, RRID:AB_11218671	
nti-Foxp3	BioLegend	Cat#320112, RRID:AB_430883	
anti-CD45	BD Horizon	Cat#561487, RRID:AB_10697046	
anti-CD11b	eBioscience	Cat#25-0112-82, RRID:AB_469588	
nti-Ly6G	BioLegend	Cat#127654, RRID:AB_2616999	
anti-Ly6C	eBioscience	Cat#17-5932-82, RRID: AB_1724153	
anti-MHC II	BioLegend	Cat#107622, RRID:AB_493727	
Anti-CD11c	eBioscience	Cat#48-0114-82, RRID:AB_2723343	
Anti-F4/80	eBioscience	Cat#12-4801-82, RRID:AB_465923	
Anti-CD206	BioLegend	Cat#141704, RRID:AB_10901166	
Anti-CD3	eBioscience	Cat#25-0031-82, RRID:AB_469572	
nti-CD4	BD Biosciences	Cat#561090, RRID:AB_10562560	
nti-CD8	BD Biosciences	Cat#560776, RRID:AB_1937317	
nti-CD44	eBioscience	Cat#17-0441-82, RRID:AB_469390	
nti-CD122	eBioscience	Cat#48-1222-82, RRID:AB_2016697	
nti-NKG2D	eBioscience	Cat#12-5885-82, RRID:AB_466005	
nti-PD-1	eBioscience	Cat#11-9985-82, RRID:AB_465472	
nti-CD45	eBioscience	Cat#367-0451-80, RRID:AB_2895962	
nti-CD49b	eBioscience	Cat#48-5971-82, RRID:AB_10671541	
nti-CD25	eBioscience	Cat#17-0251-82, RRID:AB_469366	
nti-Ki67	eBioscience	Cat#56-5698-82, RRID:AB_2637480	
nti-FoxP3	eBioscience	Cat#12-5773-82, RRID:AB_465936	
nti-CD4	BioLegend	Cat#317434, RRID:AB_2562134	
nti-CD45	BD Biosciences	Cat#564047, RRID:AB_2744403	
nti-Ki-67	BioLegend	Cat#350504, RRID:AB_10660752	
nti-CD279	Biolegend	Cat#329904, RRID:AB_940479	
nti-CD8	BioLegend	Cat#344710, RRID:AB_2044010	
nti-CD45RA	BioLegend	Cat#304126, RRID:AB_10708879	
nti-NKG2D	BioLegend	Cat#320808, RRID:AB_492962	
nti-CD45RO	BioLegend	Cat#304218, RRID:AB_493765	
nti-CD3	Thermo Fisher	Cat#47-0037-42, RRID:AB_2573936	
nti-CD25	BD Biosciences	Cat#562660,RRID:AB_2744343	
nti-FoxP3	Thermo Fisher	Cat#53-4776-42, RRID:AB_11043133	
anti-CD16	BioLegend	Cat#302016, RRID:AB_314216	
Anti-CD56	BioLegend	Cat#318316, RRID:AB_604104	
Anti-PD-1	BioXcell	Cat#BE0146, RRID:AB_10949053	
anti-CD8	BioXcell	Cat#BE0061, RRID:AB_1125541	
Anti-CD4	BioXcell	Cat#BE0003-1, RRID:AB_1107636	
IIII-0D4	DIUACEII	Gat#DEUUUS-1, KKID:AB_11U/636	

(Continued on next page)



Continued		
REAGENT or RESOURCE	SOURCE	IDENTIFIER
Anti-NK1.1	BioXcell	Cat#BE0036, RRID:AB_1107737
Anti-Ki-67	Cell Signaling	Cat#9129, RRID:AB_2687446
Anti-AE1-AE3	Santa Cruz	Cat#sc-81714, RRID:AB_2191222
Anti-CD8	Veracyte	N/A
Anti-CD3	Veracyte	N/A
Anti-NKp46	Veracyte	N/A
MACH2 rabbit universal HRP polymer	Eurobio	Cat#RHRP520L
MACH2 mouse universal HRP polymer	Eurobio	Cat#MHRP520L
MACH4 mouse universal HRP polymer	Eurobio	Cat#M4U534L
mmPACT <sup>TM</sup> AMEC Red detection	Vector Laboratories	Cat#SK-4285
Anti-CD8	Veracyte	N/A
Anti-PDL1	Veracyte	N/A
Anti-CD4	Thermo Fisher	
	THEITHOT ISHEL	Cat#17-0042-82, RRID:AB_469323
Biological samples	Cynomolaus mankaya in this attick	N/A
Cynomolgus blood Cynomolgus skin biopsy samples	Cynomolgus monkeys in this study Cynomolgus monkeys in this study	N/A N/A
	AnaPath Research S.A.U.	
Cynomolgus blood		N/A
Human blood	Patients in this study	N/A
Human tumor tissue samples	Patients in this study	N/A
Chemicals, peptides, and recombinant proteins		
LIVE/DEAD Fixable Near-IR Dead Cell Stain Kit	eBioscience	Cat#L10119
Zombie Aqua	BioLegend	Cat#423101
QIAzol Lysis Reagent	Qiagen	Cat#79306
Fixable Viability Dye eFluor <sup>™</sup> 506	eBioscience	Cat#65-0866-18
Critical commercial assays		
RNeasy Mini Kit	Qiagen	Cat#74104
Counter Mouse PanCancer Immune Profiling Panel	NanoString	Cat#115000142
Tumor Dissociation Kit	Miltenyi Biotec	Cat#130-095-929
RNeasy MinElute Cleanup Kit	Qiagen	Cat#74204
Mesoscale Discovery	Mesoscale Discovery	SN#1200120730714
RNeasy FFPE Kit	Qiagen	Cat#73504
Experimental models: Cell lines		
TRAMP-C2	ATCC	Cat#CRL-2731, RRID:CVCL_3615
TC-1	ATCC	Cat#CRL-2493, RRID:CVCL_G561
Experimental models: Organisms/strains		
C57BL/6	AnLab Co.	RRID:MGI:2159769
Mauritian cynomolgus macaques	Charles River Laboratories	N/A
Oligonucleotides		
Gene probe for CD8 Maccaca fascicularis	TIB MOLBIOL	CD8A_F: CCCTTTACTgCAACCACAggA CD8A_S: CTgCAACCACAggAACCgA CD8A_R: CTGGGCTTGCCTCCCGA
Gene probe for CD3 Maccaca fascicularis	TIB MOLBIOL	CD3E_F: ggCAggCAAAggggACA CD3E_R: CCTTTCCggATgggCTCAT CD3E_P: F-TCTgggTTgggAACAggTggTgg-C
Gene probe for actin Maccaca fascicularis	TIB MOLBIOL	bActin _L: gCgAgAAgATgACCCAgATCA bActin_R: CCTggATggCCACgTACA bActin TM: F- TTgAgACCTTCAACA CCCCAgCCA-Q

(Continued on next page)



Continued		
REAGENT or RESOURCE	SOURCE	IDENTIFIER
Software and algorithms		
FlowJo	Tree Star	Version 7.6.5
NanoStringDiff	R	Version 3.6.3
NanoString nSolver	NanoString	Version 3.0.22
DESeq2	R	Version 1.24.0
R	R	Version 3.6.3
ClusterProfiler	R	Version 4.4.4
Gene Ontology	The Gene Ontology Consortium	https://doi.org/10.1038/75556
BD FACSDivA	BD Biosciences	Version 8.0
Phoenix WinNonlin	Certara	Version 8.5
BD FACSuite	BD Biosciences	Version 1.6
NanoZoomer XR	Hamamatsu	RD15-031, RD20-023
Veracyte Digital Pathology Platform	Veracyte	EAP01-000-002-1803701
HALO	Indico Labs	Version 3.0
NanoString nCounter Analysis system	NanoString	PTL01-008
SAS	SAS	Version 9.4
Prism	GraphPad Software	Version 10.0.02

#### **EXPERIMENTAL MODEL AND STUDY PARTICIPANT DETAILS**

#### Cell culture and cell lines

TRAMP-C2 tumor cells (ATCC CRL-2731), MHC class I-deficient, were established from a heterogeneous 32-week tumor of a male transgenic adenocarcinoma mouse prostate model. TRAMP-C2 cells were maintained in D-MEM medium supplemented with 5% FCS, 5% Nu-Serum IV, 0.005 mg/mL human insulin, 10 nM dehydroisoandrosterone and antibiotics. The TC-1 tumor cell line (ATCC CRL-2493) was developed by co-transfecting male murine C57BL/6 lung cells with HPV16 E6/E7 genes and activated (G12V) Ha-ras plasmid DNA. TC-1 cells were maintained in RPMI 1640 medium supplemented with 10% FCS, 2 mM L-glutamine and antibiotics. Both cell lines were cultured at 37°C in a humidified atmosphere with 5% CO<sub>2</sub>. ATCC as a source of cell lines ensures cell authentication.

#### In vivo animal studies

#### **Mouse studies**

Studies in mice were conducted using 6–8 weeks old male C57BL/6 mice purchased from AnLab Co., Prague, Czech Republic. They were kept in individually ventilated cage systems at constant temperature ( $20^{\circ}\text{C}-24^{\circ}\text{C}$ ) and humidity (45-70%) with no more than 5 animals in each cage. The animals weighed approximately 18-22 g, were naive and underwent mandatory pathogen testing by the vendor. TRAMP-C2 ( $1\times10^6$ ) or TC-1 ( $3\times10^4$ ) tumor cells were inoculated s.c. in the flank on day 0. Before grouping and treatment, all animals were weighed and the tumor volumes were measured using calipers. In some experiments, animals were equally randomized to the experimental groups based on weight and in other experiments based on tumor volume. Animal protocols were in accordance with the laws of the Czech Republic and approved by the Czech Academy of Sciences (identification number AVCR 5345/2023 SOV II).

#### Cynomolgus monkey studies

Cynomolgus monkey studies were conducted using naive 2–4 years old 16 male and 2 female Mauritian cynomolgus macaques obtained from an established breeding facility, weighing 1.8–3.5 kg, at Charles River Laboratories, France. The animals were monitored for specific pathogens and diseases. The animals were randomized to experimental groups. The study procedures were approved by the local Institutional Animal Care and Use Committee at Charles River Laboratories, France.

All in vivo animal experiments conformed to the relevant regulatory standards.

#### **Human participants**

AURELIO-03 enrolled patients aged ≥ 18 years with selected histologically or cytologically confirmed advanced and/or metastatic solid tumors refractory or intolerant to existing therapies known to provide clinical benefit for their tumor type. ICB-naive patients and patients who experienced relapse/refractory disease on ICB therapy were eligible. Additional inclusion criteria included ECOG performance status of 0 or 1, measurable disease per iRECIST in a non-irradiated port and adequate organ system function. The main exclusion criteria were as follows: presence of untreated central nervous system metastases; additional malignancies; prior exposure to IL-2 or IL-15 agonists; history of or current diseases that interfere with ICB application; and significant cardiovascular disease, active disease or history of viral infection.

#### **Article**



Information on gender was collected at screening (female: 25 patients [49.0%], male: 26 patients [51.0%]). Patient demographic information is presented in Table S2.

This study is being conducted in compliance with the Declaration of Helsinki as revised in 2013, the International Council for Harmonisation Guidelines for Good Clinical Practice and applicable local regulatory requirements. The study was approved by the ethics committees at each participating site. All patients provided written informed consent before participation.

#### **METHOD DETAILS**

#### Reagents and antibodies

Nanrilkefusp alfa (nanril; CAS number 1416390-27-6) is a proprietary compound of SOTIO Biotech AG, Switzerland. Batches for nonclinical use were expressed in CHO-S cells and purified to ≥95% purity. The clinical batch was manufactured according to Good Manufacturing Practice specifications. Commercially available reagents and antibodies are listed in the Key Resources Table.

#### Non-clinical anti-tumor efficacy studies

Nanril was administered s.c. at 2 mg/kg in PBS or 0.9% NaCl once daily on days 4-7 and 10-13 in TC-1 tumor-bearing mice, and s.c. at 1 mg/kg once daily on days 4-7 and 18-21 in TRAMP-C2 tumor-bearing mice. For combination treatment, the anti-PD-1 antibody (clone RMP1-14 [from BioXcell]) was administered i.p. at 12.5 mg/kg on days 10, 13 and 16. Antibodies to deplete NK/CD8<sup>+</sup>/CD4<sup>+</sup> T cells (anti-CD8 clone 2.43, anti-CD4 clone GK1.5 and anti-NK1.1 clone PK 136 [all from BioXcell]) were administered i.p. at 0.1 mg/mouse on days -7, -4, -2, 4, 11 and 18. For late therapeutic experiments of established tumors, nanril was administered s.c. in the vicinity of the growing tumor at 2 mg/kg once daily on days 25-28 and 32-35 in TC-1 tumor-bearing mice (day 25 randomization  $\sim 0.1$  cm<sup>2</sup>). The depleting antibodies were administered on days 21, 24, 26 and 33. TRAMP-C2 tumor-bearing mice were administered s.c. in the vicinity of growing tumor with nanril at 1 mg/kg in PBS or 0.9% NaCl once daily on days 36-39 and 50-53 (day 36 randomization  $\sim 0.1$  cm<sup>2</sup>). All mice were observed twice per week and the size of the tumors was recorded. Two perpendicular diameters of the tumors were measured with a caliper and the tumor size was expressed as the tumor area (cm<sup>2</sup>). Tumor-free mice were re-challenged with a second inoculation of TRAMP-C2 ( $1 \times 10^6$  cells) 106 days after initial treatment.

#### Immunophenotyping and gene expression in mice

The tumors, spleens and lymph nodes were collected from 3 to 5 TC-1- or TRAMP-C2-tumor-bearing mice from 2 independent experiments 5 days after starting nanril treatment. Single-cell suspensions were prepared and analyzed by flow cytometry and NanoString. Fluorescence-activated cell sorting analyses were performed using an LSR II flow cytometer and analyzed by FlowJo 7.6.5 software. Total RNA was extracted from the tumors, spleens and inguinal lymph nodes using RNeasy Mini Kits (Qiagen). Gene expression analysis was performed using the nCounter Mouse PanCancer Immune Profiling panel (XT\_PGX\_MmV1\_CancerImm\_CSO, cat. #115000142) with a NanoString MAX system reader. Raw gene expression data were analyzed with NanoStringDiff, annotationTools packages in R and with NanoString nSolver v3.0.22 software with the Advanced Analysis Module v2.0. Differential expression was determined using DESeq2 (version 1.24.0) in R. Only genes with an adjusted p-value of  $\leq$ 0.05 were considered differentially expressed.  $\log$ 2FC  $\geq$  1 and  $\log$ 2FC  $\leq$  -1 were chosen as cutoff points for upregulated or downregulated genes, respectively. Heatmaps with hierarchical clustering analysis were assembled for DEGs using the gplots package in R software based on the Euclidean distance and complete clustering method. Functional and enrichment analyses of DEGs was performed using the ClusterProfiler and the web-based tool Gene Ontology.

#### In vitro potency assays of human PBMCs

PBMCs were obtained from buffy coats of human healthy donors (*n* = 6) by FicoII-PaquePLUS Media gradient centrifugation (Thermo Fisher Scientific). The PBMCs were cultivated in RPMI 1640 medium supplemented with 2 mM GlutaMAX I CTS, 100 U/mL penicillin, 100 mg/mL streptomycin, 1 mM sodium pyruvate, 1% non-essential amino acids, 50 mM 2-mercaptoethanol (all from Gibco) and 10% heat-inactivated AB human serum (Invitrogen). The PBMCs (10<sup>6</sup>/mL) were incubated with nanril at concentrations of 0.03, 0.1, 0.31, 0.93, 2.78, 8.33, 25 and 75 ng/mL for 7 days at 37°C in a humidified atmosphere containing 5% CO<sub>2</sub>. The following fluorescently labeled antibodies were used to label NK and CD8<sup>+</sup> T cells: CD3-APC-eFluor780, CD4-eFluor450, Ki67-APC (eBioscience), CD8-PE-DlyLight594 (Exbio), CD56-Aexa Fluor700 and CD16-PE-Cy7 (BioLegend). Dead cells detected by the LIVE/DEAD Fixable Aqua stain (Thermo Fisher Scientific) were excluded from the analyses.

#### Flow cytometry of human and mouse samples

Single-cell suspensions of spleens lysed using ammonium chloride-potassium buffer were homogenized through a cell strainer (70  $\mu$ M). Single-cell suspensions from tumors and lymph nodes were prepared using a Tumor Dissociation Kit (Miltenyi Biotec). The human PBMCs and cell suspension of mouse splenocytes, lymph node cells and tumor tissues were stained with a mixture of the appropriate extracellular antibodies and LIVE/DEAD Fixable stain (Thermo Fisher Scientific) in FACS buffer (PBS [Lonza] supplemented with 0.2% BSA [Sigma-Aldrich]) for 30 min at 4°C. After washing with FACS buffer, the cells were fixed (1 fixation concentrate: 3 fixation diluent; eBioscience) for 20 min at 4°C. Before staining with the intracellular antibodies, the cells were permeabilized with permeabilization buffer (diluted from 10× with dH<sub>2</sub>O; eBioscience). The antibodies used for the intracellular staining were



prepared in PBS containing 2  $\mu$ L of rat serum (Sigma Aldrich) and incubated for 20 min at 4°C. In mouse experiments, the samples were incubated with anti-CD16/CD32 antibody for 15 min at 4°C to minimize non-specific binding. Data were collected using Flow cytometer LSR Fortessa (Becton Dickinson) and BD DiVA software. FlowJo software (Tree Star, Inc.) was used for the cytometric data evaluation.

#### **Cynomolgus monkey studies**

In these studies, nanril was administered in 0.9% NaCl to groups of two cynomolgus monkeys by daily i.v. or s.c. injections at doses of 4, 10, 25 and 75  $\mu$ g/kg for 4 consecutive days (phase 1). One group was untreated. After a 17-day wash-out period, during phase 2, in some previously treated groups and the untreated group, nanril was administered by repeated i.v. injection at 40  $\mu$ g/kg or s.c. injection at 15  $\mu$ g/kg over 3 weeks. Blood PD was determined by flow cytometry and serum nanril concentrations were determined by ELISA. qPCR analysis of immune cells expressing CD3 $^-$ and CD8a-related genes was conducted using skin biopsies. In the 10-week PD study, the animals were administered s.c. with nanril twice weekly at 40  $\mu$ g/kg (starting on day 1) and PD was evaluated by flow cytometry of blood samples obtained on days -3, 5, 12, 19, 26, 33, 40, 47, 54, 61 and 66. Parameters monitored during the study, beyond PD and PK, included morbidity/mortality, clinical signs, local tolerance at the injection site, body temperature, body weight, clinical laboratory tests and/or determination of cytokine levels.

Skin biopsies were collected at the injection site and at a distant site 8 days after the last dose in the s.c. 2×/w and i.v. 4×/w groups and 2 days after the last administration in the s.c. 2×/w group. An untreated monkey was used as a baseline biopsy control.

For qPCR analyses, the collected biopsies, pre-chilled with liquid nitrogen, were ground to a fine powder. QIAzol lysis reagent (Qiagen) was added and mRNA was isolated by chloroform/ethanol extraction. mRNA was purified using an RNeasy MinElute Cleanup kit (Qiagen). The quantity of RNA was determined using a Nanodrop ND-1000 (Thermo Scientific) and the quality was assessed using a BioAnalyzer (Agilent Technologies–RNA 6000 Pico Chip kit). qPCR analyses were performed using gene probes for CD45, CD8 and CD3.

Freshly collected blood for PD analyses was lysed with ammonium chloride and peripheral blood mononuclear cells (PBMCs) were stained with two panels of antibodies.

The serum sampling times for cynomolgus monkeys administered nanril i.v. at 75  $\mu$ g/kg were pre-treatment, end of infusion, and at 0.5, 1.5 and 4 h post-infusion. The sampling times for monkeys administered nanril s.c. at 75  $\mu$ g/kg were pre-treatment, and 0.5, 1.5, 4, 8 and 23 h post-treatment on day 1. The sampling times for monkeys administered nanril i.v. at 4, 10 or 25  $\mu$ g/kg i.v. were pre-treatment, end of infusion, and at 2, 4, 6 and 12 h post-infusion. The sampling times monkeys administered nanril s.c. at 4, 10 or 25  $\mu$ g/kg were pre-treatment and at 1, 2, 4, 6 and 12 h post-treatment on day 1.

The sera were stored at  $-20^{\circ}$ C until required for the ELISA. The concentration of nanril was quantified using a ligand binding assay in 10% cyno serum. A rabbit antiserum, generated by immunizing rabbits with nanril batch PR01 and subsequent affinity purification, was used as the capturing agent. A commercially available biotinylated monoclonal antibody (BAM247; R&D Systems) specific to human IL-15 was used as the detection antibody. Streptavidin peroxidase was used for colorimetric readout by absorbance. The optical density was measured using Spark spectrophotometer (Tecan, Switzerland) at 450 nm and at 620 nm as a reference wavelength. Data were analyzed using Phoenix WinNonlin (Certara).

Cynomolgus monkey blood samples were obtained from AnaPath Research S.A.U. PBMCs were isolated by red blood cell lysis using ammonium chloride. The PBMCs were cultivated in RPMI 1640 medium supplemented with 2 mM GlutaMAX I CTS, 100 U/mL penicillin, 100 mg/mL streptomycin, 1 mM sodium pyruvate, 1% non-essential amino acids, 50 mM 2-mercaptoethanol (all from Gibco) and 10% heat-inactivated cynomolgus monkey human serum. PBMCs (10<sup>6</sup>/mL) were incubated with nanril at concentrations of 0.03, 0.1, 0.31, 0.93, 2.78, 8.33, 25 and 75 ng/mL for 5 days at 37°C in a humidified atmosphere containing 5% CO<sub>2</sub>. The following fluorescently labeled antibodies were used to label NK and CD8<sup>+</sup> T cells: CD45-PE-Cy7, CD3-APC-Cy7, CD4-V450, CD8-HV605, CD20-PE and Ki67-A488 (BD Biosciences). Dead cells detected using LIVE/DEAD Fixable Viable day eFluor506 (eBioscience) were excluded from the analyses.

#### **Clinical trial**

AURELIO-03 is a multicenter, open-label, phase 1/1b first-in-human clinical trial to assess the safety and tolerability of nanril administered as monotherapy and combined with pembrolizumab in patients with selected advanced/metastatic solid tumors. The dose-escalation parts were conducted in the United States, Spain, France and the Czech Republic (1 site per country). Patients were treated until disease progression, unacceptable toxicity or the patient's decision to stop treatment or withdrawal of consent. The lowest dose level (0.25  $\mu$ g/kg) was selected to represent the MABEL determined from the non-clinical studies in cynomolgus monkeys. A traditional 3 + 3 dose escalation design was followed until the MTD was reached. At each dose level, the first patient received the first cycle of nanril on days 1, 2, 8 and 9. The second and third patients were dosed  $\geq$ 7 days after the first patient's day 9, each on a different day.

The primary objectives of the dose-escalation parts of AURELIO-03 were to evaluate the safety and tolerability and to establish the MTD and/or RP2D of nanril as monotherapy and combined with pembrolizumab. The secondary objectives included determination of the PK and PD of nanril; efficacy in terms of the overall response rate, duration of response, clinical benefit rate and PFS per iRECIST; and immunogenicity.

#### **Article**



Routine safety clinical and laboratory assessments, including physical examination, vital signs, echocardiography, electrocardiography, clinical chemistry, hematology and urinalysis, were conducted at baseline and regularly until the end of study treatment. Physical examination and vital signs measurements were subsequently performed at follow-up visits every 30 days until 90 days after the last dose of nanril and/or pembrolizumab. Vital signs were closely monitored after administration of nanril. AEs were reported and coded using the Medical Dictionary for Regulatory Activities version 24.1 terminology and graded according to the National Cancer Institute Common Terminology Criteria for Adverse Events, version 5.0. The DLT evaluation period was the first 21-day treatment cycle. The MTD was defined as the dose level at which ≥33% of DLT-evaluable patients experienced a DLT. The RP2D was defined as the dose level below the MTD. The decision as to whether an AE should be considered a DLT and/or whether a dose level is to be considered intolerable was made by a dose escalation committee and endorsed by an independent advisory panel. The dose escalation committee consisted of the study investigators and the sponsor's medical monitor. The independent advisory panel comprised two independent clinical experts and an independent statistician. The radiologic tumor response was assessed by computed tomography or magnetic resonance imaging at screening and then at 6-week intervals. The PK profiles were determined using a validated mesoscale platform with a specific rabbit anti-serum to nanril.

#### **Translational analyses**

Paired tumor biopsies (archival and fresh) were collected from 16 patients in the monotherapy part and 10 patients in the combination part at baseline and in cycle 2 or at the time of progression for immunohistochemical (IHC) analysis of immune markers and gene expression profiling. Blood samples were collected at pre-dose and after treatment on days 1, 2, 6, 8, 9, 13 and 15 in cycle 1 from 27 patients in the monotherapy part and 21 patients in the combination part. Lymphocyte subsets were assessed using fresh blood samples with multiple panels of fluorescent monoclonal antibodies using a FACSLyrics' flow cytometer and BD FACSuite software (Beckton Dickinson). The serum IFN-γ levels were measured using an electrochemiluminescence immunoassay by Mesoscale Discovery on an MSD sector 6000.

Tumor specimens were fixed in neutral-buffered 10% formalin solution and embedded in paraffin per standard procedures. In brief, multiplex immunofluorescence staining was performed on 4-mm-thick formalin-fixed, paraffin-embedded (FFPE) tissue sections with Ki67 (Cell Signaling), cytokeratin (Santa Cruz) and proprietary CD8, CD3 and NKp46 (Veracyte, France) monoclonal antibodies using a Leica Bond RX. Signal detection was performed using MACH2 rabbit universal HRP polymer (Eurobio), MACH2 mouse universal HRP polymer (Eurobio) or MACH4 mouse universal HRP polymer (Eurobio) as a secondary antibody and ImmPACT AMEC Red detection (Eurobio). IHC duplex staining for PD-L1 and CD8 was performed using the Immunoscore<sub>CR</sub> IC assay (Veracyte, France) with proprietary PD-L1 (clone HDX3) and CD8 (clone HDX1) monoclonal antibodies. IHC duplex staining for CD4 and FoxP3 was performed using the Immunoscore<sub>CR</sub> SC assay (Veracyte, France) with CD4 (Thermo Fisher Scientific) and FoxP3 (eBioscience) monoclonal antibodies on Ventana Benchmark XT. Slides were scanned with a NanoZoomer XR to generate digital images (20 x). Each sample was analyzed using the proprietary Veracyte Digital Pathology Platform (Veracyte, France). Additionally, all scans were uploaded to the HALO software (Indico Labs) and analyzed using the registration and Highplex IF module. CD8-centered proximity index was calculated as the percentage of CD8+ cells located less than 20 μm from other CD8+ cells.

NanoString nCounter gene expression assay was performed using 100 ng of RNA extracted from FFPE tumor sections with an RNeasy FFPE Kit (Qiagen) followed by hybridization with code sets according to the manufacturer's recommendations. Following hybridization, the probe/target complexes were aligned and immobilized in the nCounter Cartridge and placed into the nCounter Digital Analyzer for data collection. Gene expression was analyzed using a custom Human PanCancer Immune Profiling Panel comprising 807 genes (NanoString Inc.). The mRNA counts and gene expression scores were calculated from RCC files using customized software (R version 3.6.3).

#### **QUANTIFICATION AND STATISTICAL ANALYSIS**

#### Sample size

According to the conventional 3 + 3 dose-escalation design, it was expected to include 3–6 DLT-evaluable patients per dose level, and a total of 27–54 patients was considered to be sufficient to address the study objectives.

#### Analysis sets

The safety set included all patients exposed to nanril (monotherapy part, N = 30) or nanril or pembrolizumab (combination part, N = 21). The PK analysis set included patients with an evaluable PK profile. The PD analysis set included patients with an evaluable PD profile. This patient population was used for the PK/PD analysis (monotherapy part, N = 30; combination part, N = 21). The PK evaluable analysis set was defined as all patients exposed to nanril who had a valid PK profile for at least 1 cycle and no important protocol deviation affecting PK. A valid PK profile was defined as having 1 pre-dose and at least 1 post-dose measurement. The efficacy set included all patients who were exposed to nanril for at least 1 treatment cycle and had at least 1 evaluable tumor assessment per iRECIST after the initiation of nanril treatment (monotherapy part, N = 26; combination part, N = 19). The efficacy set was used for the analysis of efficacy endpoints.



#### Statistical analyses

SAS version 9.4 was used for statistical programming.

Patient baseline characteristics and disease history were analyzed descriptively.

A non-compartmental model analysis was used to evaluate the PK parameters. All PK parameters were calculated based on the actual sampling time.

PD parameters in cycle 1 and cycle 2 were analyzed descriptively. Only samples not meeting any rule of exclusion specified in the Statistical Analysis Plan were included in the analysis. The SAS statistical package 9.4 and Prism software (GraphPad Software) were used for data management and statistical analyses. Paired t test was used in the longitudinal data analyses to compare different immune cell subsets and gene expression patterns within the same sample. Significance levels were set at 0.05 for all tests.

Any unconfirmed progressive disease per iRECIST was considered progression if it was followed by treatment discontinuation due to the lack of confirmation of progression and follow-up scans, thus deviating from the iRECIST guidelines. CR, partial response (PR), stable disease (SD), and progressive disease were identified according to iRECIST. Overall response was defined as achieving PR or CR. Disease control was defined as achieving SD, PR, or CR. SD had to last at least 6 weeks from the start of study treatment; if not, at least 1 follow-up scan assessed as PR, CR, or SD was required for disease control. Confirmation of PR or CR by a subsequent assessment of either PR or CR, at least 4 weeks apart, was required to declare an overall response of PR or CR, or disease control.

Duration of response was defined as the time since the first PR or CR until the first date of unconfirmed progressive disease per iRECIST (followed by confirmation of progression, study treatment discontinuation, or clinical progression) or death (whichever occurred earlier) for patients with confirmed PR or CR. Patients with missing data or those who received new anti-cancer therapy (other than palliative) were censored at the date of the last evaluable tumor assessment. Duration of response was summarized using Kaplan-Meier estimates.

PFS was defined as the time from the first day of study treatment until the first date of unconfirmed progressive disease per iRE-CIST (followed by confirmation of progression, study treatment discontinuation, or clinical progression) or death (whichever occurred earlier). Patients with missing data or those who received new anti-cancer therapy were censored at the date of the last evaluable tumor assessment. PFS was summarized using Kaplan-Meier estimates.

OS was defined as the time from the first day of study treatment until the date of death. Patients with missing data were censored at the last time known to be alive: apart from trial visits/survival status, information from Electronic Case Report Forms was also used to derive the survival status. The latest complete date was selected. OS was summarized using Kaplan-Meier estimates.

#### **ADDITIONAL RESOURCES**

AURELIO-03 has been registered on ClinicalTrials.gov (NCT04234113).